magnetochemistry

MDPI

Review

Ligand-Induced Self-Assembly of Clusters by Pyridine–Amine–Carboxylate Frameworks of 3D Transition Metals: Structural and Magnetic Aspects

Amit Rajput [1], Akram Ali [2], Himanshu Arora [3,*] and Akhilesh Kumar [4,*]

[1] Department of Chemistry, J. C. Bose University of Science & Technology, YMCA, Faridabad 121006, Haryana, India
[2] Department of Chemistry, Chowdhary Mahadev Prasad College, University of Allahabad, Prayagraj 211002, Uttar Pradesh, India
[3] Department of Chemistry, University of Allahabad, Prayagraj 211002, Uttar Pradesh, India
[4] Department of Chemistry and Nano Science, Ewha Womans University, Seoul 03760, Republic of Korea
* Correspondence: himanshuarora@allduniv.ac.in (H.A.); akhiliitk2012@ewha.ac.kr (A.K.)

Abstract

The ligand-driven self-assembly of metal clusters offers a powerful strategy for constructing discrete molecular architectures with tunable magnetic and structural properties. By judiciously selecting appropriate multidentate ligands, researchers can direct the formation of polynuclear metal assemblies with diverse nuclearities, geometries, and topologies. Coordination-driven processes commonly stabilize such assemblies where multidentate ligands operate as templates and linkers. These will also determine how the metal centers are arranged in space and how they connect to each other. These clusters can take on shapes that range from basic bridging dimers to more complicated icosahedral and cubane-type motifs. They often have excellent symmetry and strong frameworks. Magnetically, these clusters are a great place to study exchange interactions, spin frustration, and the behavior of single-molecule magnets (SMMs). The magnetic characteristics depend on things like the type of metal ions, the bridging ligands, the overall shape, and the local coordination environment. Interestingly, a large number of ligand-assembled clusters exhibit high spin ground states and slow magnetization relaxation, which makes them attractive options for quantum information storage and molecular spintronic devices. This review connects coordination chemistry, supramolecular design, and molecular magnetism of pyridine–amine–carboxylate frameworks, offering insights into fundamental magnetic phenomena and guiding the development of next-generation functional materials. Continued exploration of ligand frameworks and metal combinations holds the potential to yield novel clusters with enhanced or unprecedented magnetic characteristics.

Keywords: 2-pyridyl-alkylamine-carboxylate ligands; polymeric cluster; discrete cluster; magnetic properties; magnetostructural correlation

Check for updates

Academic Editors: Boris Tsukerblat and Andrew Palii

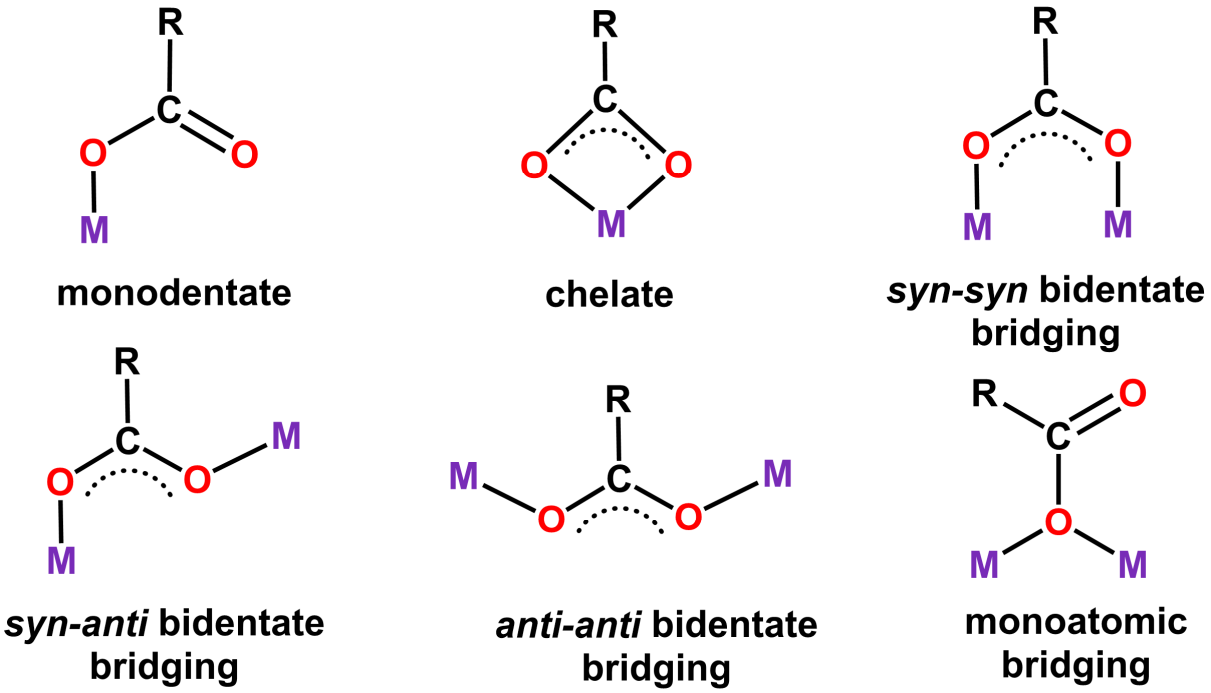
Received: 13 October 2025
Revised: 21 January 2026
Accepted: 30 January 2026
Published: 4 February 2026

Copyright: © 2026 by the authors. Licensee MDPI, Basel, Switzerland. This article is an open access article distributed under the terms and conditions of the Creative Commons Attribution (CC BY) license.

1. Introduction

Alfred Werner, in 1893, introduced the concept of octahedral structures for transition metal complexes, laying the groundwork for determining their coordination numbers and oxidation states, thereby explaining the behavior of the double salts of that era [1]. The term originated from the observation that transition metal ions bond not only to anionic ligands but also to extra species beyond charge neutrality. This discovery laid the foundation

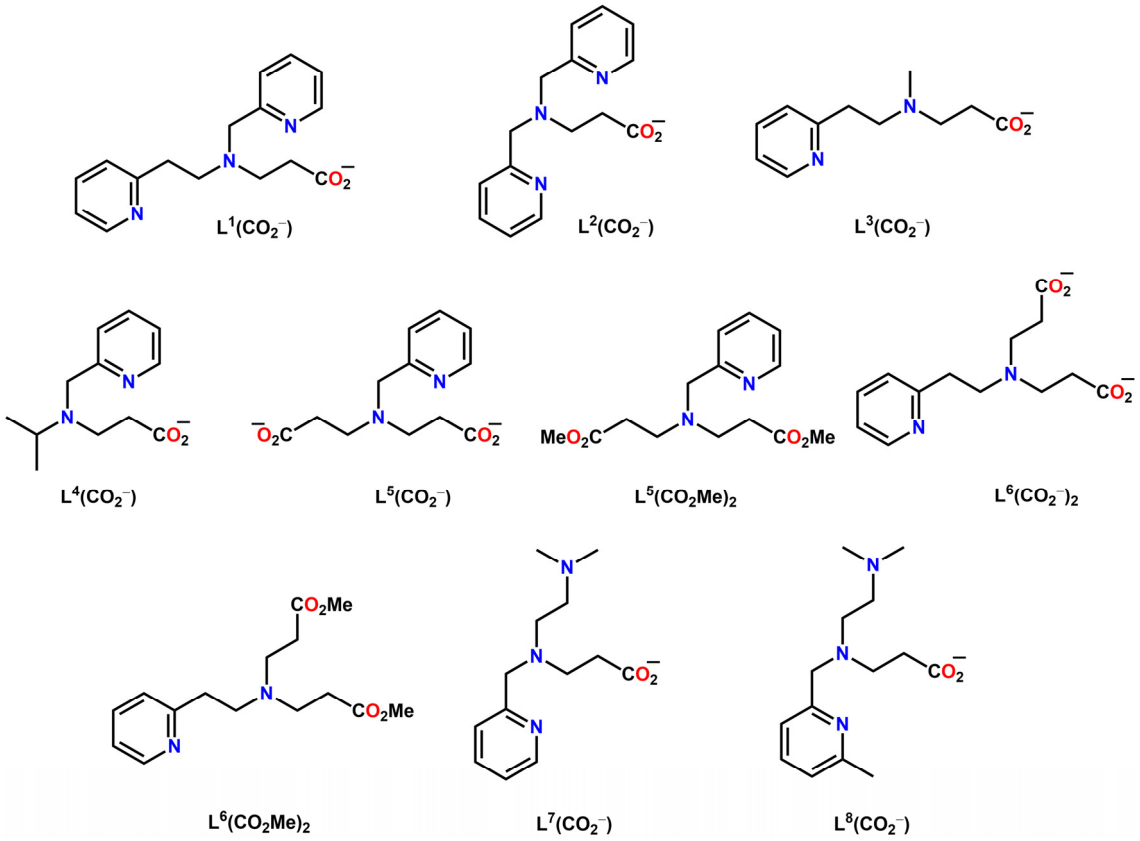
of modern coordination chemistry, enabling rational design of metal–ligand complexes with defined geometries. Over the past century, coordination chemistry has advanced remarkably, deepening our understanding of metal–ligand complexes, structures, and reactivity. Recently, the field has expanded to include metal–organic frameworks (MOFs) and supramolecular coordination complexes (SCCs) [2]. In the past two decades, the domain of polynuclear and discrete clusters has progressed significantly [3–23]. Metal ions (connectors) and specially designed organic ligands (linkers) are used to create polynuclear and discrete clusters. Transition metal ions with diverse coordination geometries serve as versatile connectors [3–5,19,20] and impart coordination clusters with many characteristics, including magnetic and catalytic ones. They can therefore be employed as versatile functional materials that play a pivotal role in modern crystal engineering, where the rational design and assembly of molecular building blocks enable the creation of materials with tailored structures and properties [3–5,19,20]. Extensive structural analysis of coordination clusters reveal that transition metal ions have coordination either from the O-atoms of anions (carboxylates, phosphates, nitrates, sulphates, and phenolates) or the N-atoms of pyridines, amines, cyanates, or cyanides [11–16]. These statistics underscore the significance of pyridine-carboxylate moieties in the formation of coordination clusters, emphasizing how their diverse coordination behavior and electronic properties facilitate the generation of multidimensional frameworks with enhanced structural stability and potential functional applications in catalysis, magnetism, and molecular recognition [21–23]. Notably, carboxylate groups can adopt a variety of bridging conformations, the most notable of which are triatomic *syn-syn*, *syn–anti*, *anti-anti*, and monoatomic [24–26]. The *syn-syn* conformation encourages the creation of binuclear systems, whereas *syn–anti* promotes the formation of extended structures with fluctuating nuclearity. Because of their diverse bridging capacities, carboxylates are suitable linkers between metal ions for the propagation of metal-ligand coordination units (Scheme 1).



Scheme 1. The monodentate and bidentate chelating mode and bridging conformations of carboxylate groups.

The (2-pyridyl)alkylamine moiety is widely recognized as a ligand in coordination chemistry in general, and in bioinorganic chemistry in particular, [27–46]. In this review

article, we present coordination complexes synthesized from a systematically diversified class of (2-pyridyl)alkylamine-appended carboxylate functionalities (Scheme 2). The bridging coordination mode of the carboxylate, limited by the coordination of the (2-pyridyl)alkylamine moiety to a metal ion, facilitates the prediction of the propagation direction.



Scheme 2. The ligands pertinent to this article.

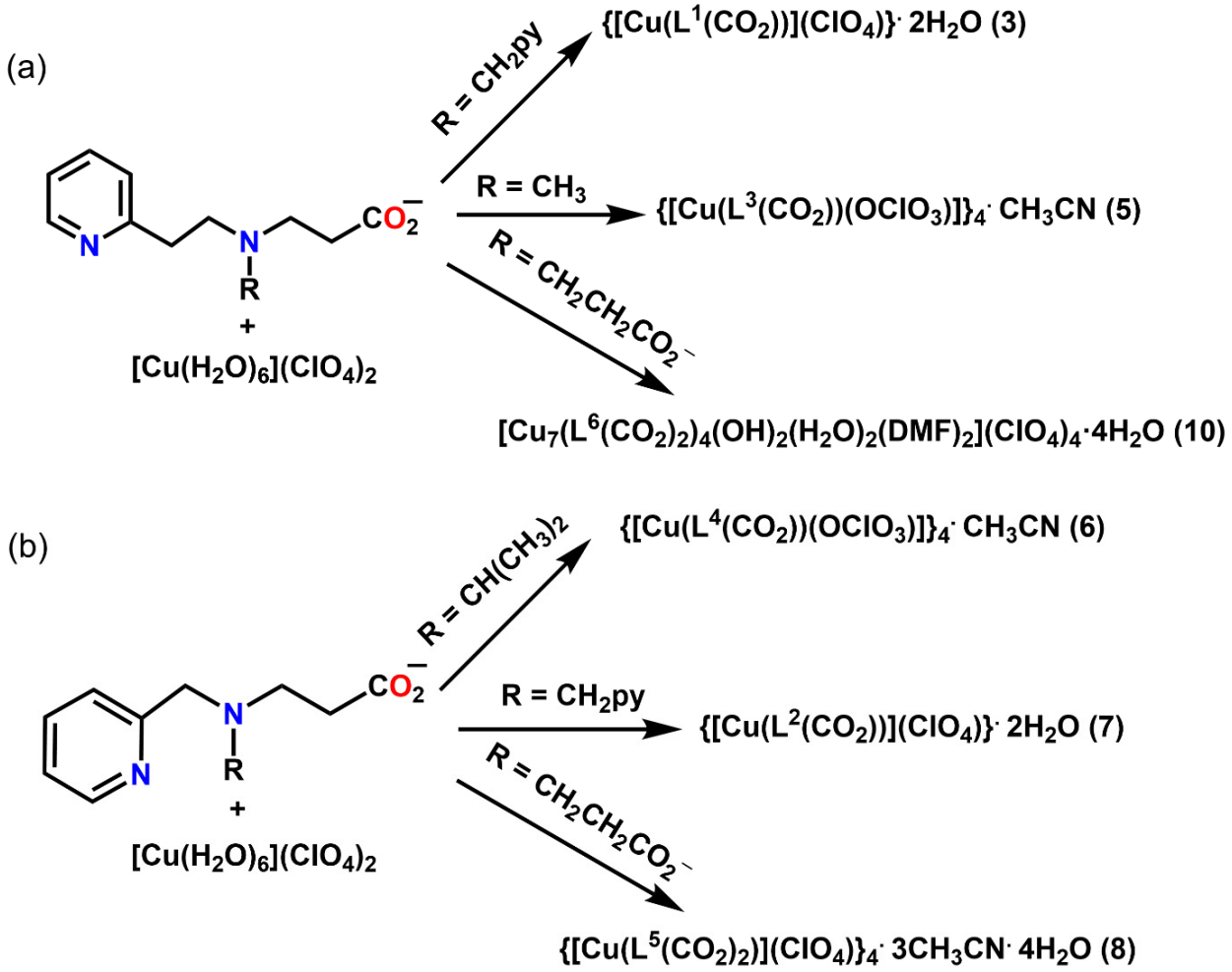
It is important to note that (2-pyridyl)alkylamine-appended carboxylate ligands (Scheme 2) make "rigid" metal–ligand coordination units, even though they are versatile because the methylene spacer between the N2/N3 chelating donor sites and the carboxylate functionality can change. It has been very helpful to use the selected ligands (Scheme 2) that integrate the two functional groups in order to synthesize discrete di-, tetra-, and multi-metallic cores (see Scheme 1) as well as new coordination polymers (see Scheme 1).

2. Ligand Impact on Self Assembly of Coordination Cluster

2.1. Ligand Denticity Influence

Very few reports are available in the literature where researchers have pointed out that one can change the nuclearity of the self-assembly of coordination complexes with ligand denticity. Mukherjee and coworkers have reported that when they took 2-pyridylalkylamine appended carboxylate-based ligands of different denticities, one can change the nuclearity of the final coordination complexes (Schemes 3–5). The reaction of the tetradentate ligand, $L^1(CO_2^-)$ with metal salts (where the metals are manganese, cobalt, copper, zinc) leads to coordination polymers {$[Mn^{II}(L^1(CO_2))(H_2O)](ClO_4)\cdot 2H_2O$ (**1**) [47], $[Co^{II}(L^1(CO_2))(H_2O)](ClO_4)\cdot 2H_2O$ (**2**) [48], $[Cu^{II}(L^1(CO_2))](ClO_4)\cdot 2H_2O$ (**3**) [48], $[Zn^{II}(L^1(CO_2))](ClO_4)\cdot 2H_2O$ (**4**) [47]}, but when one arm of the ligand (CH_2py or CH_2CH_2py) is detached and denticity is reduced by one unit, i.e., $L^3(CO_2^-)/L^4(CO_2^-)$; tridentate ligand, one can synthesize discrete tetranuclear units ({$[Cu(L^3(CO_2))(OClO_3)]$}$_4\cdot$ CH_3CN (**5**) and {$[Cu(L^4(CO_2))(OClO_3)]$}$_4\cdot CH_3CN$ (**6**)) (in the case of copper) (Scheme 3) [49].

The findings presented herein highlight the fundamental role of ligand denticity as a powerful design parameter in directing metal–ligand self-assembly. Notably, even subtle variations in coordination mode can profoundly alter assembly pathways, shifting outcomes from extended polymeric frameworks to well-defined discrete clusters. This level of control over nuclearity has significant implications for the rational design of coordination materials, as it enables precise modulation of structural dimensionality and metal aggregation—critical factors governing the magnetic, catalytic, and functional properties of coordination complexes.

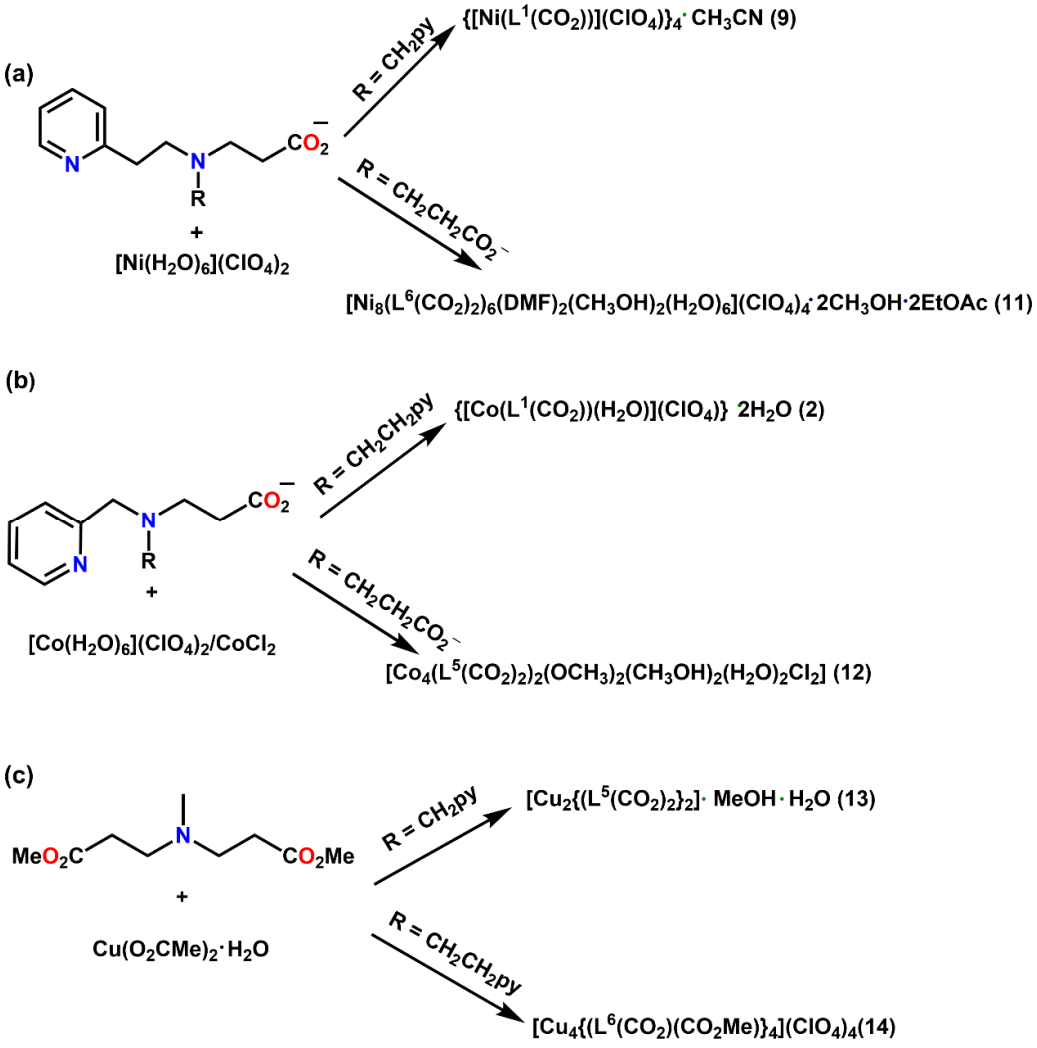


Scheme 3. Schematic representation of ligand denticity and flexibility influence (**a**) for $L^1(CO_2)$; $L^3(CO_2)$; $L^6(CO_2)^2$ (**b**) for $L^4(CO_2)$; $L^2(CO_2)$; $L^5(CO_2)_2$.

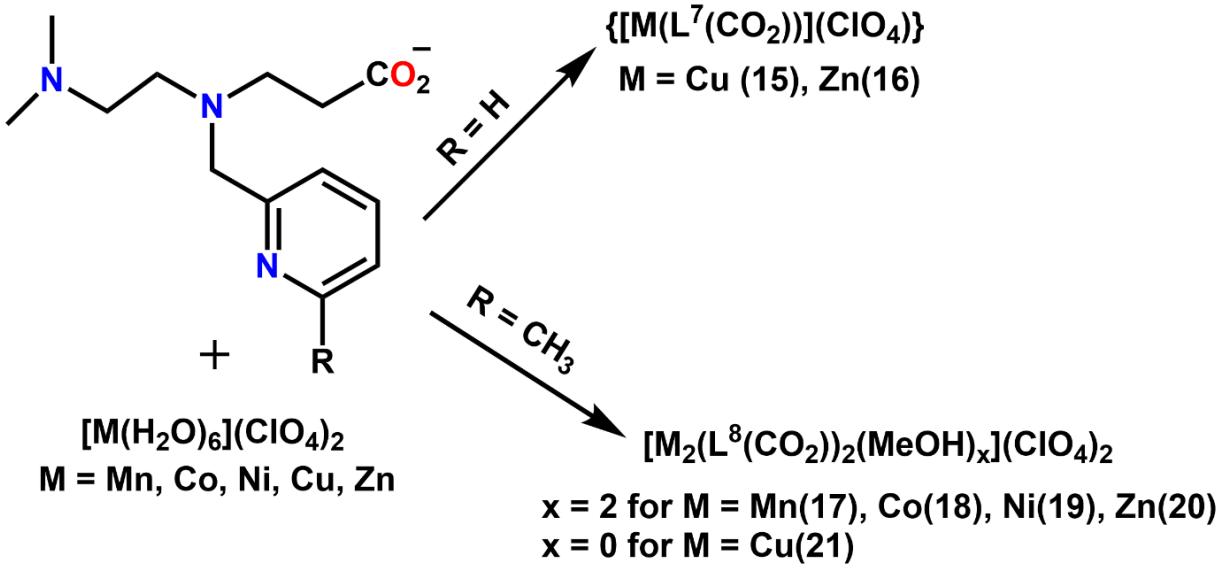
2.2. Ligand Flexibility Influence

Mukerjee and coworkers have reported that if one can introduce more flexibility in the ligand, replacing the CH_2py arm in $L^5(CO_2^-)_2$ with the more flexible CH_2CH_2py in $L^6(CO_2^-)_2$, one can play with nuclearity. The reaction of $L^5(CO_2^-)_2$ with copper yields a tetranuclear cluster [49] while $L^6(CO_2^-)_2$ with copper yields a heptanuclear cluster (Scheme 4) [50]. Arora et al. have also reported that replacing the CH_2py arm in $L^1(CO_2^-)$ with more flexible $CH_2CH_2(CO_2^-)$ in $L^6(CO_2^-)_2$, one can double the nuclearity. The reaction of $L^1(CO_2^-)$ with nickel yields a tetranuclear cluster [49] while $L^6(CO_2^-)_2$ with nickel yields an octanuclear cluster [51]. A similar pattern was observed for $L^2(CO_2^-)$ and $L^5(CO_2^-)_2$. The reaction of tetradentate ligand $L^2(CO_2^-)$ with copper leads to a coordination polymer [52], while with $L^5(CO_2^-)_2$ copper gives discrete tetranuclear unit [49]. It

is worth noting that in the case of cobalt, one can change the nuclearity if we change the metal salt. The reaction of tetradentate ligand $L^1(CO_2^-)$ with cobalt $\{[Co(H_2O)_6](ClO_4)_2\}$ leads to coordination polymer [48], while the reaction of $L^5(CO_2^-)_2$ with cobalt $\{CoCl_2\}$ gives discrete tetranuclear unit [53]. Mukherjee and coworkers recently reported that reaction of $L^5(CO_2Me)_2$ with $Cu(O_2CCH_3)_2{\cdot}H_2O$ leads to a discrete dinuclear complex, while the reaction of more versatile $L^6(CO_2Me)_2$ with $[Cu(H_2O)_6](ClO_4)_2$ leads to a discrete tetranuclear cluster [54]. The observations reported here highlight a broader design strategy in coordination chemistry, wherein fine control over ligand flexibility and arm length enables predictable modulation of nuclearity and assembly outcomes. By tailoring ligand adaptability, it becomes possible to steer systems toward specific cluster sizes or to suppress extended frameworks altogether. This insight is particularly significant for the rational construction of metal clusters with tunable nuclearity, offering pathways to optimize structure-dependent properties such as magnetism, reactivity, and functional performance in coordination-based materials.



Scheme 4. Schematic representation of ligand flexibility influence (**a**) for Nickel complexes (**b**) for Cobalt complexes (**c**) for Copper Complexes.



Scheme 5. Schematic representation of ligand bulk influence.

2.3. Steric Bulk Influence

Kaur and Manda et al. have reported that introducing steric bulk in the form of a methyl group next to the pyridine-N in ligand $L^7(CO_2^-)$ can convert the polymeric system into a discrete unit. Reaction of $L^7(CO_2^-)$ with metals (manganese, cobalt, copper and zinc) leads to a coordination polymer [47,48], while reaction of $L^8(CO_2^-)$ with metals (manganese, cobalt, copper, and zinc) leads to discrete dinuclear complex (Scheme 5) [55,56]. The results reported here emphasize the broader implication that steric engineering at strategic ligand positions offers an effective tool for directing self-assembly pathways and nuclearity. By modulating spatial congestion near donor sites, one can deliberately switch between extended frameworks and discrete metal clusters. This insight provides a valuable design principle for tailoring coordination architectures, enabling rational control over structure-dependent properties in functional coordination materials.

3. Magneto-Structural Features of the Systems and the Underlying Structure–Property Trends

There are numerous factors, such as the coordination geometry preferred by metal ions, conformation of chosen ligands, the solvent system, influence of counterions, the reaction temperature, sometimes ligand-to-metal stoichiometry [21–23], that govern the self-assembly [11–16] of organic chelating ligands and inorganic metal ions to create coordination cluster network topology. The primary characteristics of linkers and connectors are the alignment and quantity of their binding pockets, which correspond to coordination geometries and coordination numbers, respectively. The chemical characteristics of organic ligands are crucial in determining the framework of coordination clusters [21–23], as they bind the metal centers and transmit the structural information reflected in metal coordination preferences across the extended structure.

The predictability of the network geometry of coordination clusters (polymeric or discrete) remains a difficult problem, despite the fact that a number of coordination clusters have been studied to date and many useful functional properties have been discovered [9]. We now provide a snapshot of magneto-structural attributes (structure–property relationships) of coordination clusters, which can be either discrete or polymeric, that were created sequentially employing the ligands $L^1(CO_2^-)$ to $L^8(CO_2^-)$. Most coordination complexes, whether polymeric or discrete, that utilize carboxylate ligands with (2-pyridyl)-alkylamine attached fall within the one-dimensional (1D) structure (see below). The main explanation

might be the way the selected ligands coordinate with a specific metal ion and an extra bridging carboxylate O to link to the nearest neighbor (tridentate: one pyridyl N, one amine N, and a carboxylate O; tetradentate: two pyridyl N, one amine N, and a carboxylate O or one pyridyl N, one amine N, and two carboxylate O). Therefore, the creation of either discrete multimetallic clusters or 1D coordination polymers is encoded by the type of ligand donor atoms. One or more solvent molecules may complete the coordination sphere in response to a specific metal ions coordination need.

It is apt to mention here that ligands $L^3(CO_2^-)$, $L^4(CO_2^-)$, $L^5(CO_2Me)_2$, $L^6(CO_2Me)_2$, $L^6(CO_2^-)_2$ and $L^8(CO_2^-)$ have not afforded so far any coordination polymers; instead, the formation of discrete carboxylate-bridged clusters (dimer, tetramer, heptamer or octamer) has been accomplished [48–51,53–56]. Notably, $L^1(CO_2^-)$ generates both a discrete tetramer [49] as well as a 1D coordination polymer (see Figure 1) [48].

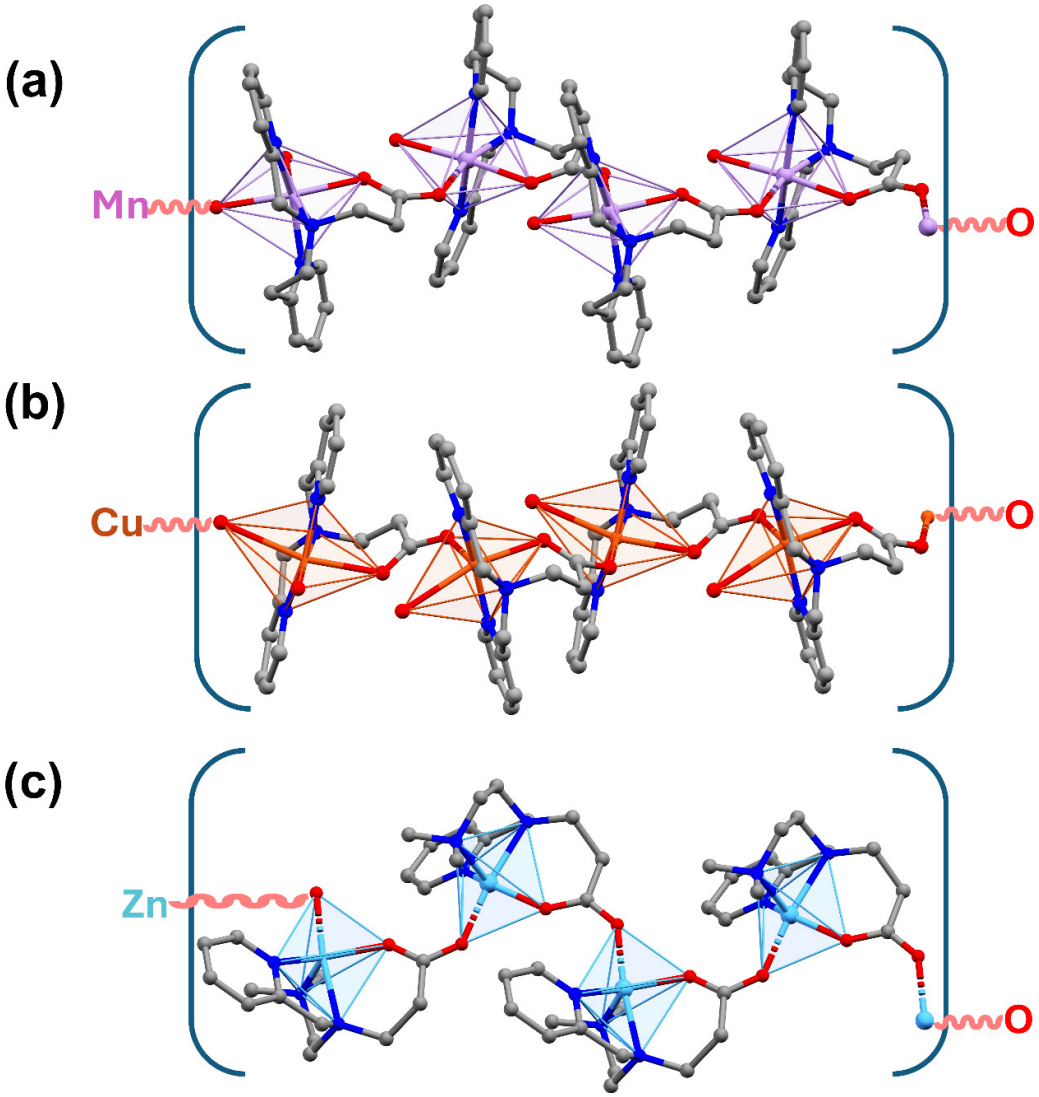


Figure 1. Schematic representation of polyhedral view of 1-D coordination polymers (**a**) **1**, (**b**) **7** and (**c**) **16**. Color code: violet, Mn; orange, Cu; cyan, Zn; blue, N; red, O; and gray, C atoms. Reproduced with permission from ref. [47]. Copyright 2001, John Wiley and Sons.

To further understand the magnetic exchange interactions, temperature-dependent magnetic susceptibility measurements were performed on chosen instances from the given systems. The chosen systems exhibit both ferromagnetic and antiferromagnetic behavior (energy gap between singlet and triplet states expressed in terms of J in cm^{-1}; magnetic

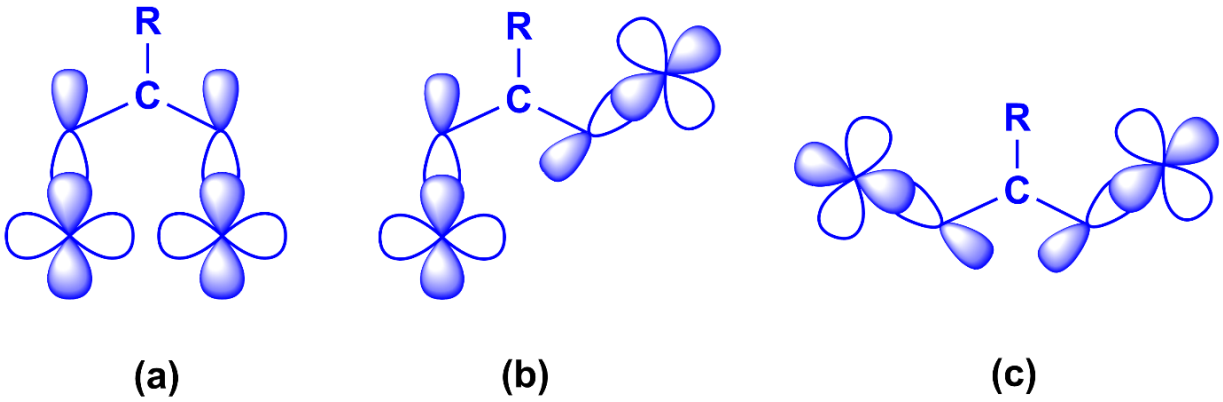
exchange coupling constant (J) is negative for antiferromagnetic and positive for ferromagnetic interactions between two adjacent metal centers), as well as spin-canting behavior (see below).

3.1. Coordination Polymers

The potential tetradentate ligands $L^1(CO_2^-)$, $L^2(CO_2^-)$ and $L^7(CO_2^-)$ afforded the carboxylate-bridged 1D polymeric chain complexes $[Mn^{II}(L^1(CO_2))(H_2O)](ClO_4)\cdot 2H_2O$ (**1**) [47], $[Co^{II}(L^1(CO_2))(H_2O)](ClO_4)\cdot 2H_2O$ (**2**) [48], $[Cu^{II}(L^1(CO_2))](ClO_4)\cdot 2H_2O$ (**3**) [48], $[Zn^{II}(L^1(CO_2))](ClO_4)\cdot 2H_2O$ (**4**) [47], $[Cu^{II}(L^2(CO_2))](ClO_4)\cdot 2H_2O$ (**7**) [52], $[Cu^{II}(L^7(CO_2))](CF_3SO_3)\cdot H_2O$ (**15**) [47], and $[Zn^{II}(L^7(CO_2))](ClO_4)$ (**16**) [47]. The M(II) ions are successively bridged by *syn–anti* carboxylate groups (Table 1). In **1**, two nitrogen (ethylpyridyl and methylpyridyl), one carboxylate oxygen from the ligand, and another oxygen from water form the basal plane. An oxygen atom from the carboxylate group of a neighboring molecule and the nitrogen of a tertiary amine from the ligand facilitate axial coordination, thereby achieving six-coordination around the manganese. In **1**, extensive π–π stacking [47] involving alternate pyridine rings of adjacent 1D chains exists, which eventually leads to the formation of a 2D network structure. In **2**, one tertiary amine nitrogen, two carboxylate oxygens, one within the ligand and another from an adjacent molecule, and oxygen from water form the basal plane. Ethylpyridyl and methylpyridyl nitrogens provide axial coordination, and hence complete six-coordination around the cobalt. In **3**, **7,** and **15**, the three nitrogen atoms of the ligand and the oxygen atom belonging to the carboxylate of an adjacent molecule form the basal plane. The oxygen atom of the carboxylate present within the ligand as an axial ligand completes five coordination around the copper. In each case, the copper(II) center exhibits a distorted [τ = 0.01 (**3**), 0.19 (**7**) and 0.19 (**15**); values of 0 and 1 are indicative of idealized square-pyramidal and trigonal-bipyramidal geometries, respectively] [57] square-pyramidal CuN_3O_2 coordination geometry. The bridging carboxylate is in axial–basal (or axial–equatorial) mode. In $[Zn^{II}(L^7(CO_2))](ClO_4)$ (**16**) [47], the Zn(II) ion displays a distorted trigonal–bipyramidal coordination geometry (τ = 0.60) [57] The basal coordination plane consists of two nitrogen donors and a carboxylate oxygen atom from $L^7(CO_2^-)$, whereas the apical sites are occupied by a carboxylate oxygen atom of an adjacent ligand and the tertiary amine nitrogen donor from $L^7(CO_2^-)$. Perspective views of **1**, **7** and **16** are shown in Figure 1. From the figure, it is apparent that all of them have *syn–anti* carboxylate O–C–O bridges. Temperature-dependent magnetic susceptibilities for **1**, **3**, **7** and **15** revealed very weak antiferromagnetic/ferromagnetic interactions through *syn–anti* carboxylate bridges between the M^{II} centers [J = -0.25 cm^{-1} (**1**), -0.66 (1) cm^{-1} (**3**), +0.14 cm^{-1} (**7**) and -1.88 (1) cm^{-1} (**15**)] (Table 1) [47,48,52].

A comprehensive evaluation of the magneto-structural data for carboxylato-bridged coordination polymers [25,47,48,52,58,59] permits the following generalizations. In the *syn–syn* conformation, the exchange interaction is strongly antiferromagnetic, attributable to the short metal–metal separation and efficient overlap of the magnetic orbitals. In contrast, the *syn–anti* conformation gives rise to very weak, and in some instances, ferromagnetic exchange, whereas the *anti–anti* conformation typically results in weak to moderate antiferromagnetic coupling. Intuitively, the magnetic coupling constant (J) can be expected to be the sum of both ferromagnetic (J_F) and antiferromagnetic (J_{AF}) contributions [60]. In examining magneto-structural trends, the copper(II) systems provide a representative case. For *syn–anti* conformations, both weak ferromagnetic and weak antiferromagnetic couplings have been reported [26,47,48,52,59]. The nature of the coupling is governed by the structural characteristics of the Cu–O–C–O–Cu′ bridging unit, which modulates the extent of magnetic orbital overlap. The non-planarity of this unit is expected to reduce the overlap, which, in turn, is expected to favor ferromagnetic exchange coupling [26,47,48,52,59]. The

nature and extent of coupling also depend on the coordination geometry of the Cu(II) centers. For a square planar/square pyramidal geometry, the ground state of the Cu(II) ion is described by the $d_{x^2-y^2}$ orbital, and for a trigonal bipyramidal geometry, the relevant metal orbital is d_{z^2} [48]. For the basal–basal (or equatorial–equatorial) *syn–anti* conformation, the contributions between the 2p orbitals of the O and O′ atoms belonging to the magnetic orbitals centered on Cu and Cu′ are unfavorably oriented to give a significant overlap (Scheme 2) [26,47,48,52]. Under these conditions, $J_{AF} \approx 0$, resulting in the predominance of weak ferromagnetic interactions. In cases where *syn–anti* carboxylate bridges connect an equatorial site of one Cu(II) center to the axial site of an adjacent Cu(II) center, the magnetic orbital of the Cu(II) ion in a square-pyramidal environment ($d_{x^2-y^2}$) acquires partial admixture of the d_{z^2} orbital characteristic of a trigonal-bipyramidal geometry [48]. The resulting magnetic exchange is expected to be extremely weak, as it involves interaction between a $d_{x^2-y^2}$ orbital and a d_{z^2} orbital, the latter contributing only a minimal spin density [47]. This unfavorable orientation of the magnetic orbitals centered on the Cu(II) ions accounts for the weak ferro-/antiferromagnetic coupling (Scheme 6) [26,47,48,52]. In the light of the structural trends and the orbital interaction considerations discussed above, the nature and extent of magnetic interaction through the *syn–anti* carboxylate bridge observed in Cu(II) coordination polymers (**3**, **7** and **15**) can readily be rationalized [47,48,52]. Complexes **3** and **15** show weak antiferromagnetic coupling [−0.66 (1) cm^{-1} (**3**) and −1.88 (1) cm^{-1} (**15**)] (Figure 2) while **7** shows ferromagnetic coupling [+0.14 cm^{-1} (**7**)]. For **3**, **7** and **15**, the small overlap between the magnetic orbitals of the Cu(II) ion through the syn–anti carboxylato bridge (in both it is an axial–equatorial bridge) for a Cu–O–C–O–Cu′ skeleton that is not planar [dihedral angle values: **3**, ~3°; **7**, ~31°; **15**, ~22°], the dihedral angles of the carboxylate group coordinated to Cu′ and the CuN_3O plane (**3**, ~86°; **7**, ~78°; **15**, ~67°], and the Cu···Cu distance [**3**, 4.579 (6) Å; **7**, 5.800 (2) Å; **15**, 5.281 (9) Å], account for the weak antiferromagnetic/ferromagnetic coupling observed [47,48,52].



Scheme 6. The orbital interaction between the metal ion ($d_{x^2-y^2}$-type orbital) and the carboxylate group in (**a**) *syn–syn*, (**b**) *syn–anti* and (**c**) *anti–anti* bridging mode. Reproduced with permission from ref. [55]. Copyright 2021, Royal Society of Chemistry.

Complex **2**, the only *syn–anti* carboxylate–bridged Co(II) coordination polymer, exhibits clear spin-canted antiferromagnetism [20,48]. Magnetic measurements reveal spontaneous magnetization below ~5 K (Figure 3), consistent with weakly antiferromagnetic coupling [$J = -2.65$ (2) cm^{-1}] (Figure 4) [20,48] This behavior arises when structural asymmetry prevents strict antiparallel alignment of neighboring spins [60–63], leading to a small canting angle and weak ferromagnetism. In **2**, the Co(II) centers deviate appreciably from ideal octahedral geometry and are connected through markedly non-planar syn–anti carboxylate bridges (Co–O–C–O–Co′ dihedral ≈ 13.7°) [48]. The absence of an inversion center between adjacent Co(II) ions, combined with strong single-ion spin–orbit coupling ($\lambda \approx -163$ cm^{-1}) and zero-

field-splitting-induced anisotropy [61], results in unequal easy-axis orientations. Consequently, magnetic measurements show a small remanent moment (Mr ≈ 0.019 μB), a coercive field of ~200 G, and an estimated canting angle of ~0.5°, which together provide unambiguous experimental evidence for spin-canted antiferromagnetism in complex **2** [60–63].

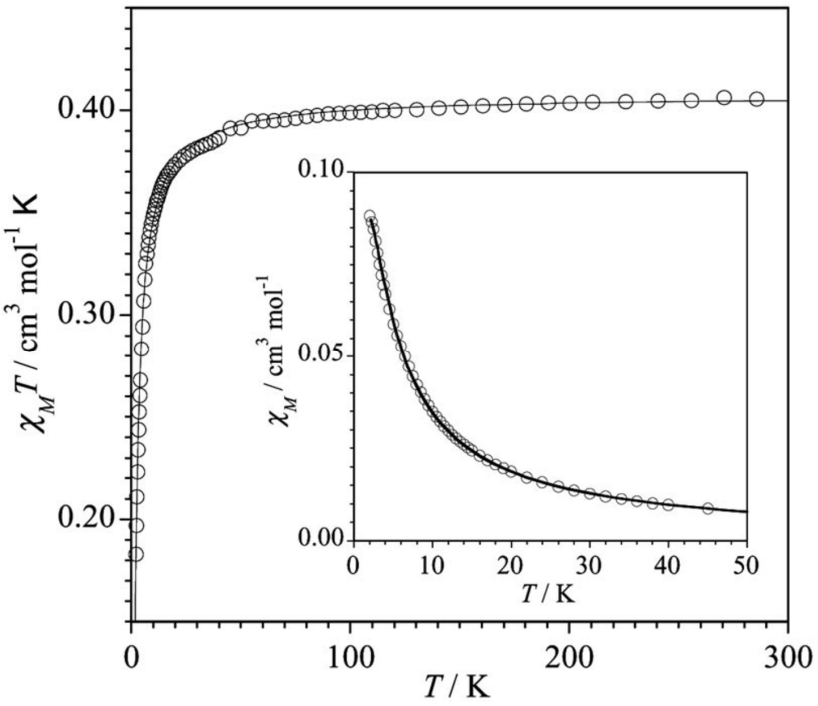


Figure 2. Plot of $\chi_M T$ vs. T for a powdered sample of $[Cu^{II}(L^7(CO_2))](CF_3SO_3)\cdot H_2O$ (**15**). The solid lines represent the best theoretical fit, described in the text. The plot of χ_M vs. T is in inset. Reproduced with permission from ref. [47]. Copyright 2001, John Wiley and Sons.

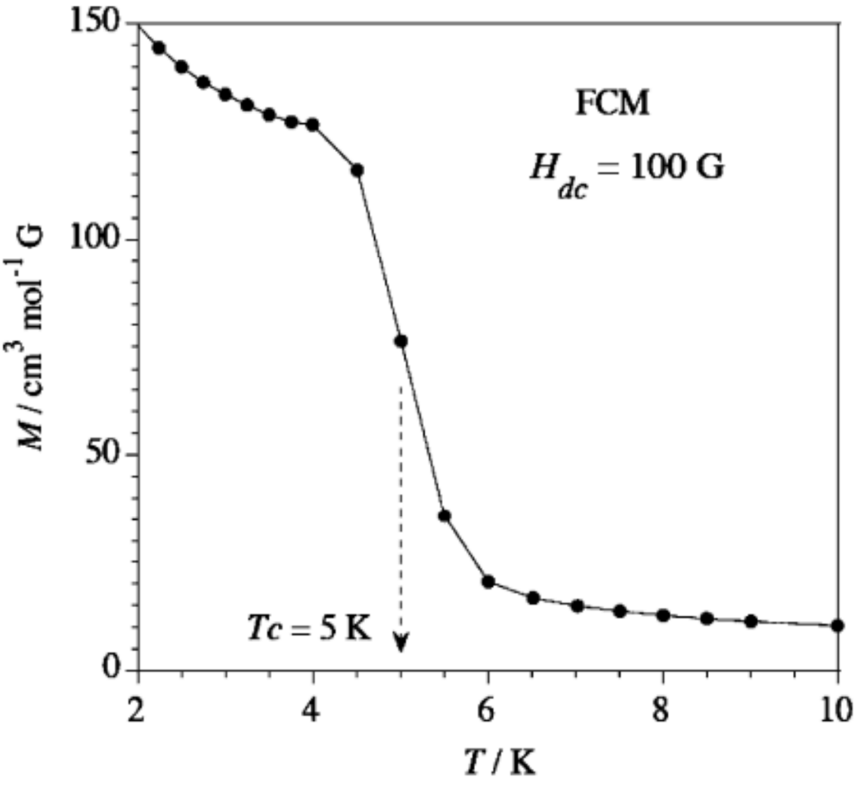


Figure 3. The field-cooled magnetization of $[Co^{II}(L^1(CO_2))(H_2O)](ClO_4)\cdot 2H_2O$ (**2**). Reproduced with permission from ref. [48]. Copyright 2009, American Chemical Society.

Table 1. Summary of Structural and Magnetic Features of Complexes.

System Type	Complexes (No.)	Metal Ion (s)	Nuclearity/Topology	Dominant Bridging Mode	Coordination Geometry (Metal)	Magnetic Behavior	Exchange Coupling *J* (cm^{-1})/Key Feature
1D coordination polymers	**1–4**, **7**, **15**, **16**	Mn^{2+}, Co^{2+}, Cu^{2+}, Zn^{2+}	Infinite 1D chains	*syn–anti* carboxylate	Mn/Co: distorted octahedral; Cu: square-pyramidal; Zn: trigonal-bipyramidal	Very weak AFM (Antiferromagnetic)/FM (Ferromagnetic)	$J \approx -0.25$ (1), -0.66 (3), $+0.14$ (7), -1.88 (15)
Spin-canted polymer	**2**	Co^{2+}	1D polymer	*syn–anti* carboxylate (non-planar)	Distorted octahedral	Spin-canted antiferromagnetism	$J \approx -2.65$; weak ferromagnetism below ~5 K
Tetranuclear clusters (Cu/Ni squares)	**5**, **6**, **8**, **9**, **14**	Cu^{2+}, Ni^{2+}	M_4 square/16-membered ring	*syn–anti* carboxylate	Square-pyramidal	Weak ferromagnetic	$J \approx +11$ to $+13$ (Cu_4); $+1.2$ (Ni_4)
Tetranuclear Co cluster	**12**	Co^{2+}	Defective dicubane	μ-1,1-carboxylate + μ_3-OCH_3	Distorted octahedral	Predominantly AFM (multiple pathways)	$J_1 = +3.3$, $J_2 = -2.5$, $J_3 = +10.6$
Heptanuclear cluster	**10**	Cu^{2+}	Body-centered antiprismatic Cu_7	Carboxylate + μ_3-OH	Mixed (octahedral and square-pyramidal)	Overall antiferromagnetic	*J* range: -183 to $+23.4$
Octanuclear cluster	**11**	Ni^{2+}	Distorted cubane Ni_8	*syn–anti*, *anti–anti*, monodentate carboxylate	Distorted octahedral	Overall antiferromagnetic	Mixed: J = +0.6 to -24.4
Binuclear complexes (dimers)	**13**, **17–21**	Mn^{2+}, Co^{2+}, Ni^{2+}, Cu^{2+}	M_2	*syn–anti* carboxylate	Mn/Co/Ni: octahedral; Cu: square-pyramidal	Metal-dependent AFM/FM	AFM: Mn ($J = -1.47$), Co ($J = +0.840$); FM: Ni ($J = +2.95$), Cu (+3.43)

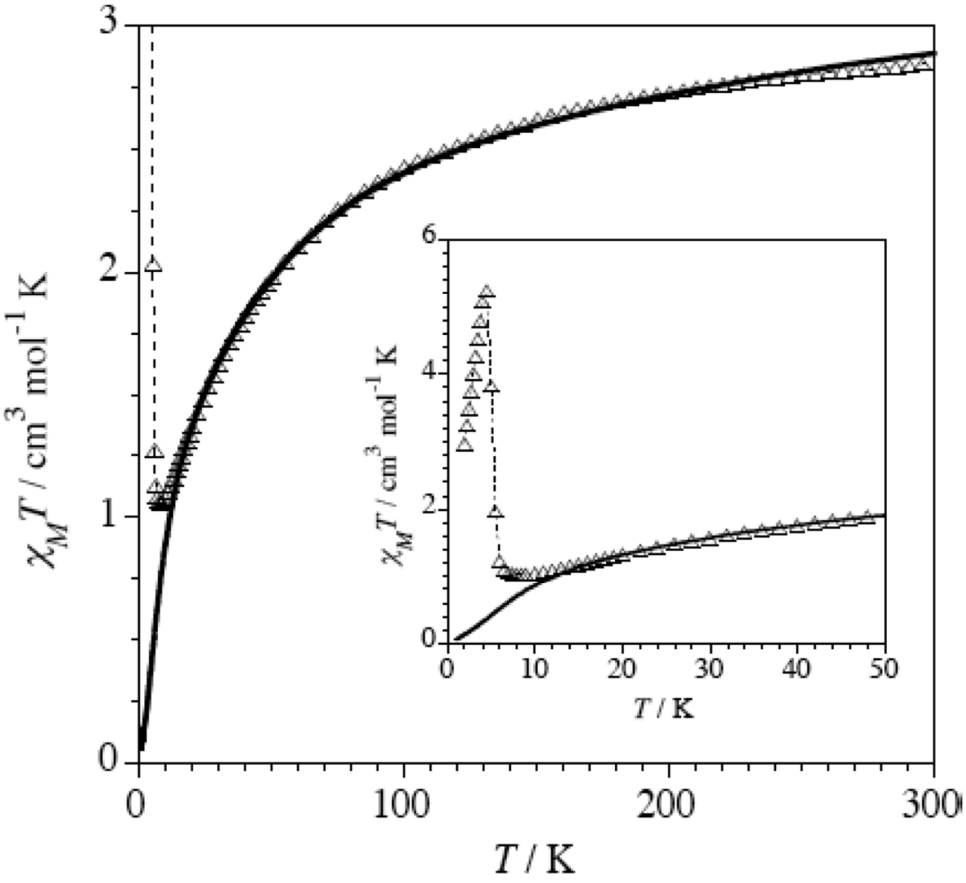


Figure 4. A plot of $\chi_M T$ vs. T for a powdered sample of $[Co^{II}(L^1(CO_2))(H_2O)](ClO_4)\cdot 2H_2O$ (**2**). Inset: expanded view of the dependence of the $\chi_M T$ product of **2** in the low temperature (<10 T) region under 0.01 T. Reproduced with permission from ref. [48]. Copyright 2009, American Chemical Society.

3.2. Discrete Clusters

3.2.1. Tetramers

The potential tridentate ligands $L^3(CO_2^-)$, $L^4(CO_2^-)$ and tetradentate ligands $L^5(CO_2^-)_2$, $L^1(CO_2^-)$ and $L^6(CO_2Me)_2$ afforded the carboxylate bridged discrete tetranuclear coordination complexes $\{[Cu(L^3(CO_2))(OClO_3)]\}_4\cdot CH_3CN$ (**5**) [48], $\{[Cu(L^4(CO_2))(OClO_3)]\}_4\cdot CH_3CN$ (**6**) [49], $\{[Cu(L^5(CO_2)_2)](ClO_4)\}_4\cdot 3CH_3CN\cdot 4H_2O$ (**8**) [49], $\{[Ni(L^1(CO_2))](ClO_4)\}_4\cdot CH_3CN$ (**9**) [49], $[Co_4(L^5(CO_2)_2)_2(OCH_3)_2(CH_3OH)_2(H_2O)_2Cl_2]$ (**12**) [53], $[Cu_4\{L^6(CO_2)(CO_2Me)\}_4](ClO_4)_4$ (**14**) [54]. X-ray analysis reveals that complexes **5**, **6**, **8**, **9**, **12** and **14** are discrete *syn–anti* carboxylate-bridged tetranuclear species. Complexes **5** and **6** comprise four "$\{Cu(L^{3/4}(CO_2))(OClO_3)\}$" units linked by tridentate carboxylate ligands, while complexes **8**, **9** and **14** are built from four "$\{Ni(L^1(CO_2)\}^+$/$\{Cu(L^5(CO_2)_2\}^+$/$\{Cu(L^6(CO_2)(CO_2Me)\}^+$" units interconnected through tetradentate carboxylate ligands. It should be noted that each $L^6(CO_2Me)_2$ is coordinated in its partially hydrolyzed $L^6(CO_2^-)(CO_2Me)$ form (Figure 5) as a tetradentate ligand to each Cu(II) ion in **14**. The carboxylate-bridging groups and four M(II) ions form a 16-membered ring $(–M–O–C–O)_4$ (M = Ni, Cu) with the metal ions located at the corners of an approximate square plane (Figure 5b). The Ni···Ni separations are ~6.25 Å along the flattened edges and ~4.50 Å along the others, with distances including van der Waals radii. This is true for all cases except **12**. The M(II) center assumes an ideal square-pyramidal geometry {τ = 0.100 (**5**), τ = 0.180 (**6**), and τ = 0.001 (**9**)} [57]. The corresponding distortion parameters for complex **14** are 0.010, 0.080, 0.012, and 0.055. This is due to the unsymmetrical structure of **14**. The tetranuclear structure of **12** can be thought of as being formed with two "$Co\{L^5(CO_2)_2\}Cl$" units connected by "$\{Co_2(OCH_3)_2(CH_3OH)_2(H_2O)_2\}$" units through two μ_3-OCH_3 and

two μ-1,1-carboxylate bridges (Figure 6a). Thus, four dimeric units {Co1(μ-1,1-OCO-)(μ_3-OCH_3)Co2}$^{2+}$, {Co1(μ-1,1-OCO-)(μ_3-OCH_3)Co2#}$^{2+}$, {Co1#(μ-1,1-OCO-)(μ_3-OCH_3)Co2}$^{2+}$ and {Co2(μ_3-OCH_3)$_2$Co2#}$^{2+}$ are formed. The four Co(II) ions are located at four corners of a defective dicubane (two cubanes sharing one face and each missing one vertex, see Figure 6b).

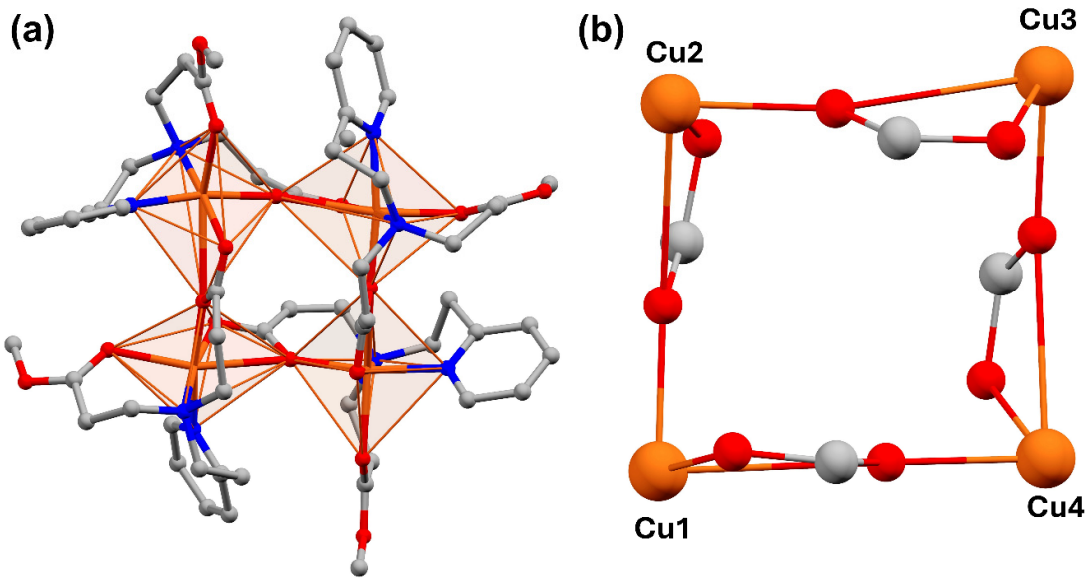


Figure 5. (**a**) Perspective view of metal coordination environment in **14** and (**b**) Tetranuclear core. Color code: orange, Cu; blue, N; red, O; and gray, C atoms. Reproduced with permission from ref. [54]. Copyright 2023, Elsevier.

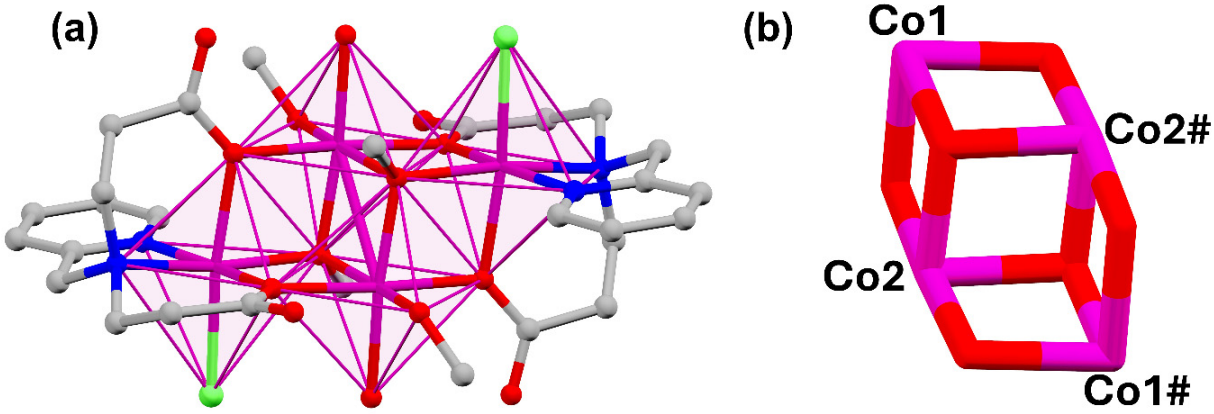


Figure 6. (**a**) Schematic representation of polyhedral view of metal coordination environment in **12** and (**b**) Defective cubane core. Color code: Green, Ni; Pink, Co; blue, N; red, O; and gray, C atoms. Reproduced with permission from ref. [53]. Copyright 2023, Royal Society of Chemistry.

The global feature of the magnetic behavior of **5**, **6**, **8**, **9,** and **14** (Figure 7; Table 1) is characteristic of a weak ferromagnetic exchange interaction, arising from intramolecular interactions between the four M^{II} ions. The best-fit parameters are g = 2.08, $D_{S=2}$ = 0.8 cm^{-1}, and J = 12.2 cm^{-1} for **5**, g = 2.10, $D_{S=2}$ = 0.4 cm^{-1}, and J = 11.1 cm^{-1} for **6**, g = 2.07, $D_{S=2}$ = 0.35 cm^{-1}, and J = 13.4 cm^{-1} for **8**, g = 2.18, $D_{S=4}$ = 3.34 cm^{-1}, and J = 1.2 cm^{-1} for **9,** and g = 2.09, $D_{S=2}$ = 0 cm^{-1}, and J = 13.1 cm^{-1} for **14** [48,49,53]. The J values obtained here are comparable to reported systems of similar structural type [64–67]. In all these systems, the *syn–anti* carboxylato bridge favors ferromagnetic interactions. As illustrated in Scheme 7a, the magnetic orbitals are oriented in a manner that precludes significant overlap, thereby leading to ferromagnetic coupling. Additionally, the non-planarity of the

M–O–C–O–M bridging framework further diminishes orbital overlap, enhancing the ferromagnetic contribution. All these features have been analyzed through DFT calculations for Cu(II) complexes for different conformations of the carboxylate bridge [68]. The calculated *syn–anti* coupling constant (~10 cm^{-1}) aligns closely with our experimental results, and the strong magnetic exchange in **5**, **6**, **8**, and **14** is attributed to carboxylate bridges linking adjacent equatorial positions (Scheme 7a). In order to understand the different nature of the magnetic exchange interactions in these Cu^{II}_4 complexes (ferromagnetic), it is important to take into account the fact that the *syn–anti* carboxylate bridge mediates weak magnetic-exchange interactions, either ferro- or antiferromagnetic [26,69–74]. Scheme 7b illustrates that when the α angle approaches 90°, ferromagnetic exchange is favored, whereas smaller angles promote antiferromagnetic coupling. This prediction agrees with the observed α values (~71.77° for **5** [48], 71.84° for **6** [49], ~73.86° for **8** [49], and 81.70° for **14** [54]). Out-of-plane deviations in the M–O–C–$O^{\#}$–$M^{\#}$ framework (vide supra) also contribute significantly. Variable-temperature magnetic studies reveal anti-ferromagnetic coupling in **12** (Table 1) [53]. Three magnetic exchange interactions (one anti-ferromagnetic and two ferromagnetic: J_1 = +3.3 cm^{-1} (Co···Co 3.176 Å; μ-1,1-OCO- and μ_3-OCH_3 bridges), J_2 = −2.5 cm^{-1} (Co···Co 3.228 Å; μ_1-OCO- and μ_3-OCH_3 bridges) and J_3 = +10.6 cm^{-1} (Co···Co 3.084 Å; two μ_3-OCH_3 bridges)) have been identified, with the inclusion of the orbital reduction parameter (α = Aκ = 1.38), spin–orbit coupling (λ = −158 cm^{-1}) and axial distortion (energy gap Δ = −975 cm^{-1} between singlet and doublet levels), rationalized by density functional theory (DFT) calculations. The computational part of the magnetic study employs ab initio wavefunction methods to understand the magnetic anisotropy by explicitly evaluating the spin–orbit coupling (SOC) of complex **12**. Using CASSCF/NEVPT2 [75–77] calculations on each metal center, the authors computed the zero-field splitting (ZFS) tensor (D-tensor), which governs anisotropic magnetic behavior. The magnetic exchange interactions in the tetranuclear cluster were treated within the Heisenberg–Dirac–van Vleck framework, with coupling constants evaluated using broken-symmetry DFT following the methodology of Ruiz and co-workers [78,79]. Calculations were performed on the full experimental geometry using Gaussian 09 and the magnetic data were analyzed using an effective spin Hamiltonian incorporating first-order spin–orbit coupling via the T–P isomorphism formalism, implemented in XVPMag. Spin-only approaches such as Kambe, irreducible tensor operator, or Magpack methods were avoided due to strong anisotropy. Kambe's method [80] is a classical approach for analyzing exchange-coupled polynuclear systems, based on successive spin coupling under the assumption of equivalent or symmetry-related exchange interactions. By rewriting the isotropic Heisenberg–Dirac–van Vleck Hamiltonian [78,79] in terms of total and intermediate spin operators, it enables analytical or semi-analytical expressions for the energy levels in terms of spin quantum numbers. The method is most effective for highly symmetric clusters, such as rings, cubes, or tetrahedra, where magnetic centers are related by symmetry and exchange constants are identical or fall into a few symmetry-distinct classes. This allows a direct correlation between structure, symmetry, and magnetic properties. However, its applicability is strongly limited by symmetry requirements. In low-symmetry systems, including distorted clusters, mixed-metal compounds, or coordination polymers with inequivalent exchange pathways, Kambe's assumptions break down. Additionally, the method is restricted to isotropic exchange and cannot readily treat anisotropy. As a result, its practical use is confined to idealized, highly symmetric systems.

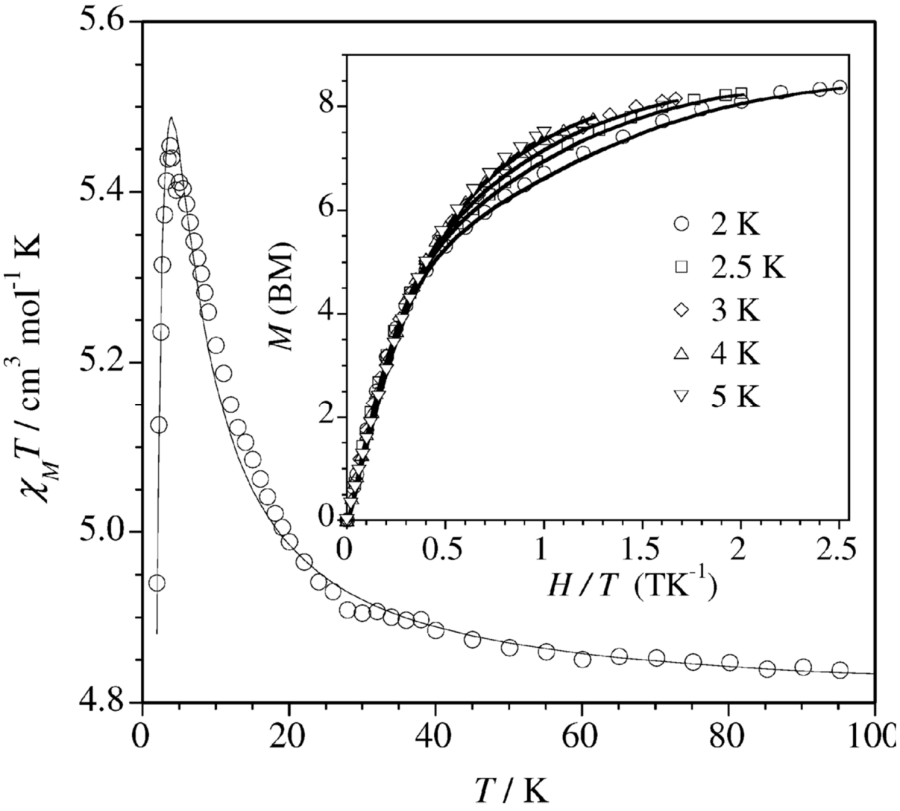
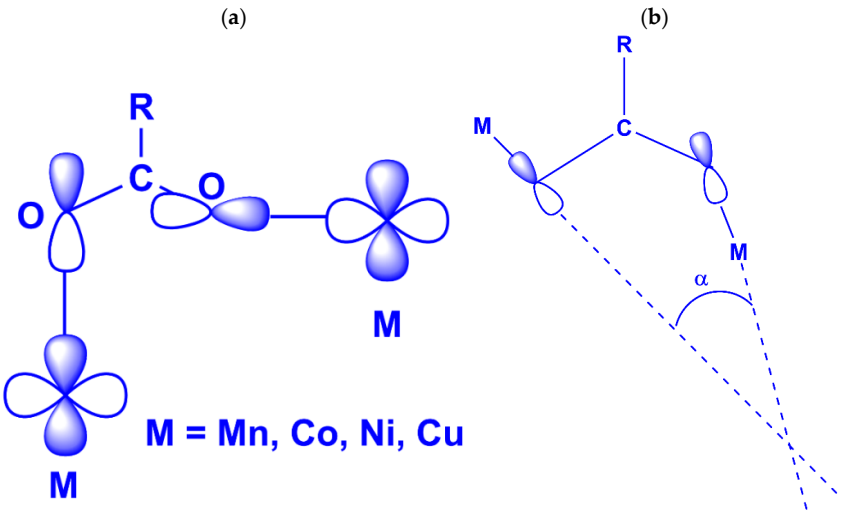


Figure 7. Plot of $\chi_M T$ vs. T for a powdered sample of 9. The inset sows the magnetization vs. applied field at 2.0, 2.5, 3.0, 4.0 and 5.0 K. The solid lines represent the best theoretical fits described in the text. Reproduced with permission from ref. [49]. Copyright 2009, Royal Society of Chemistry.



Scheme 7. (**a**) The *syn–anti* bridging conformation for the carboxylate group. (**b**) The *syn–anti* bridging conformation of the carboxylate group is characterized by an angle of α. Reproduced with permission from ref. [55]. Copyright 2021, Royal Society of Chemistry.

The elevated χMT values arise from unquenched orbital angular momentum of octahedral Co(II) (^4T_1g), with SOC-induced Kramers doublets quantitatively described by α, λ, and Δ parameters. The SOC operator mixes low-lying excited states with the ground state, and this mixing—quantified through tensorial matrix elements—directly generates the axial (D) and rhombic (E) components of the ZFS tensor. These tensor operators were used to reconstruct the full *g*-tensor and to analyze the principal magnetic axes, allowing the authors to identify the origin of anisotropy and magnetic relaxation pathways. The

interplay between SOC tensor contributions and the ligand-field–split electronic states provided a detailed, quantitative explanation of the experimentally observed magnetic behavior. Magnetic data were analyzed over the entire temperature range using Equation (1), which describes the coupling between the orbital angular momentum (L) and the spin angular momentum (S). To account for magnetic interactions between the paramagnetic centers, the spin Hamiltonian in Equation (2) was employed, assuming that these interactions are sufficiently weak and operate only when the ground Kramers doublet of each Co(II) ion is predominantly populated. Under this approximation, each paramagnetic center can be represented as an effective spin ($S_{\text{eff}} = 1/2$) with a temperature-dependent g_{eff} value, obtained by applying the spin–orbit coupling Hamiltonian (H_{SOC}) described in Equation (1). By combining the $\hat{H}_{\text{exchange}}$ and $\hat{H}_{\text{Zeem-eff}}$ Hamiltonians (Equations (2) and (3)), the best-fit parameters found through the XVPMag software (v2001) are $A\kappa = 1.38$, $\lambda = -158\ \text{cm}^{-1}$, $\Delta = -975\ \text{cm}^{-1}$, $J_1 = +3.3\ \text{cm}^{-1}$, $J_2 = -2.5\ \text{cm}^{-1}$, and $J_3 = +10.6\ \text{cm}^{-1}$. A second-order SOC model was further applied to each Co(II) ion, where the local $S = 3/2$ ground state exhibits significant zero-field splitting (D) as defined in Equation (4).

$$\hat{H}_{SOC} = -\alpha\lambda\hat{L}\cdot\hat{S} + \Delta[\hat{L}_z^2 - \frac{1}{3}L(L+1)] + \beta H[g_e\hat{S} - \alpha\hat{L}] \quad (1)$$

$$\begin{aligned}\hat{H}_{\text{exchange}} = &-J_1(\hat{S}_{\text{Co1}}\cdot\hat{S}_{\text{Co2}} + \hat{S}_{\text{Co1}^{\#}}\cdot\hat{S}_{\text{Co2}^{\#}}) \\ &- J_2(\hat{S}_{\text{Co1}}\cdot\hat{S}_{\text{Co2}^{\#}} + \hat{S}_{\text{Co1}^{\#}}\cdot\hat{S}_{\text{Co2}}) - J_3\hat{S}_{\text{Co2}}\cdot\hat{S}_{\text{Co2}^{\#}} \\ &+ g\beta H(\hat{S}_{\text{Co1}} + \hat{S}_{\text{Co2}} + \hat{S}_{\text{Co1}^{\#}} + \hat{S}_{\text{Co2}^{\#}})\end{aligned} \quad (2)$$

$$\hat{H}_{\text{Zeem-eff}} = g^{\text{eff}}\beta H(\hat{S}^{\text{eff}}_{\text{Co1}} + \hat{S}^{\text{eff}}_{\text{Co2}} + \hat{S}^{\text{eff}}_{\text{Co1}^{\#}} + \hat{S}^{\text{eff}}_{\text{Co2}^{\#}}) \quad (3)$$

$$\hat{H}_{\text{zfs}} = D[\hat{S}_z^2 - \frac{1}{3}S(S+1)] \quad (4)$$

3.2.2. Heptamer

The potential tetradentate ligand $L^6(CO_2^-)_2$ afforded a mixed carboxylate and hydroxo-bridged discrete heptanuclear coordination complex $[Cu^{II}_7(L^6(CO_2)_2)_4(\mu_3\text{-OH})_2(H_2O)_2(DMF)_2](ClO_4)_4\cdot 4H_2O$ (**10**) [50]. The structure of **10** is unique and consists of a centrosymmetric carboxylato- and hydroxo-bridged heptanuclear copper(II) cation, with body-centered anti-prismatic topology (Figure 8). The four crystallographically independent copper(II) centers exhibit pronounced differences in coordination geometry. Cu4 adopts an elongated octahedral geometry with an equatorial CuO_4 plane and two weakly bound axial carboxylate O atoms, whereas Cu1 and Cu2 display CuN_2O_3 square-pyramidal coordination, and Cu3 exhibits a CuO_5 square-pyramidal environment. The three copper(II) ions from the central centrosymmetric fragment are held by two carboxylato- and two hydroxo-bridging ligands in the equatorial positions of Cu4. Beyond confirming the cluster's authenticity, structural analysis of complex **10** highlights two key features: the presence of a $\{Cu^{II}_3(\mu_3\text{-OH})\}^{5+}$ core and a hydrogen-bonded network involving a metal-bound carboxylate and a coordinated water molecule, with the latter serving as a proton donor. Both features bear biological significance, and, in particular, the $\{Cu^{II}_3(\mu_3\text{-OH})\}^{5+}$ unit observed in **10** is relevant to understanding copper's role in multicopper oxidases [81] as well as in model studies [82,83].

Magnetic measurements reveal that in this unprecedented cluster, the net magnetic exchange is antiferromagnetic (Figure 9). The magnetic-exchange coupling constants (J values) used in the analysis exhibit a range of magnitudes, reflecting the specific geometric parameters of the interacting Cu(II) centers (Scheme 8). Five magnetic exchange interactions

(one anti-ferromagnetic and four ferromagnetic: J_1 = –183 (2) cm^{-1}, J_2 = +23.4 (5) cm^{-1}, J_3 = +8.3 (3) cm^{-1}, J_4 = +7.9 (2) cm^{-1}, J_5 = +1.3 (2) cm^{-1}, g = 2.15 (1)) have been identified [55]. A uniform g value ($g\| = g\perp = g$) was assumed for all seven Cu(II) centers. Notably, for **10**, the J values derived from B3LYP-level DFT calculations show excellent agreement with the experimental data [50].

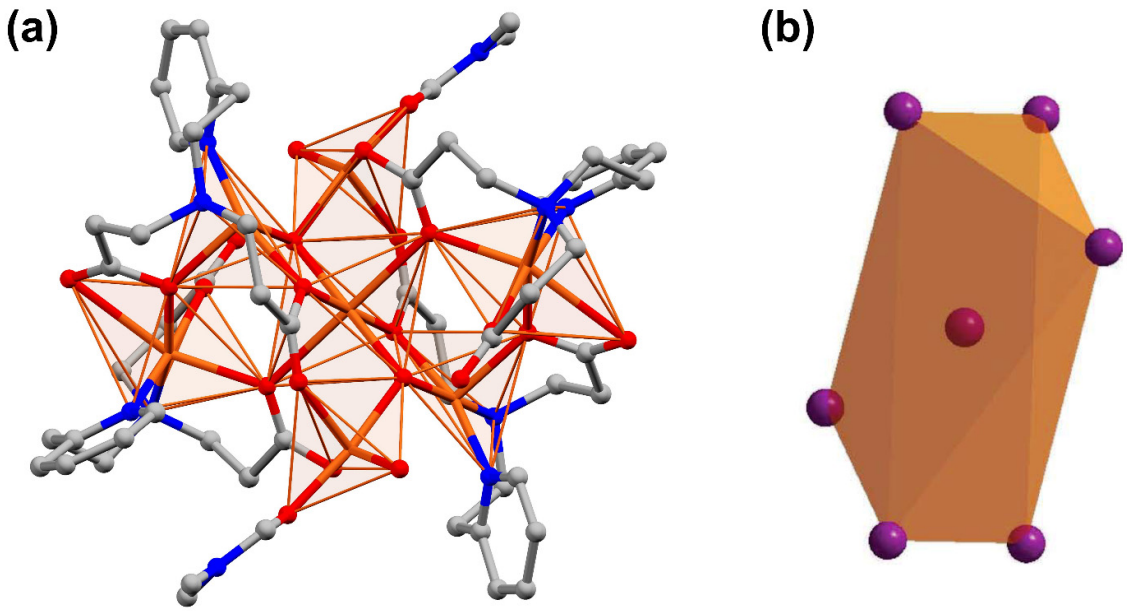


Figure 8. (**a**) Schematic representation of polyhedral view of metal coordination environment in **10**. (**b**) Antiprismatic cage formed by seven coppers. Color code: orange, Cu; blue, N; red, O; and gray, C atoms. Reproduced with permission from ref. [50]. Copyright 2011, Royal Society of Chemistry.

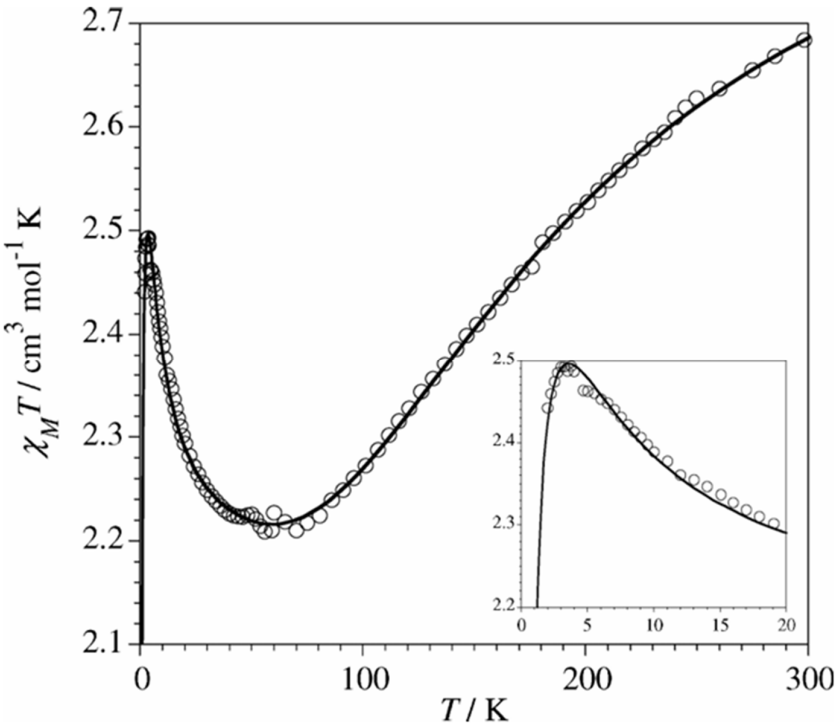
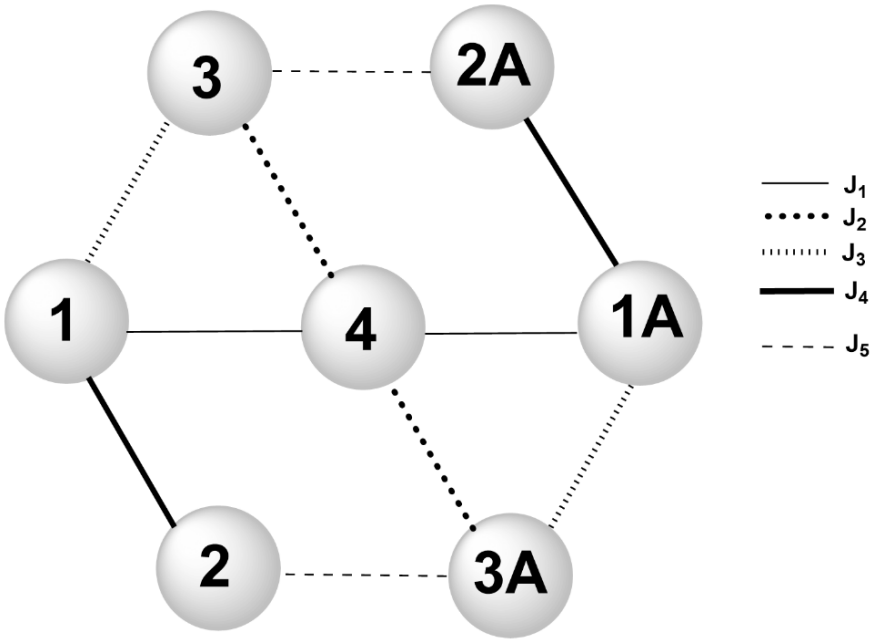


Figure 9. The temperature dependence of $\chi_M T$ for **10**. The inset shows the maximum of $\chi_M T$ for **10**. Reproduced with permission from ref. [50]. Copyright 2011, Royal Society of Chemistry.



Scheme 8. A scheme showing the topology of the spin–spin exchange interactions in cluster **10**. Reproduced with permission from ref. [50]. Copyright 2011, Royal Society of Chemistry.

3.2.3. Octamer

The potential tetradentate ligand $L^6(CO_2^-)_2$ afforded carboxylate-bridged discrete octanuclear coordination complex $[Ni^{II}_8(L^6(CO_2)_2)_6(DMF)_2(CH_3OH)_2(H_2O)_6](ClO_4)_4 \cdot 2CH_3OH \cdot 2CH_3CO_2C_2H_5$ (**11**) through 'coordination-driven self-assembly'. A deformed cubane topology and a centrosymmetric octanuclear carboxylate-bridged nickel(II) tetracation are revealed by the crystal structure of **11** [51]. The coordination environment of all nickel ions are distorted octahedron with coordination mostly coming from ligand $L^6(CO_2^-)_2$, except for Ni4 where coordination is satisfied mostly by solvent molecules. Acetates in **11** are present in three bridging coordination modes: monatomic (μ_2-1,1-bridge), *syn–anti* (μ_2-1,3-bridge), and *anti–anti* (μ_2-1,3-bridge). The octanuclear nickel(II) core has a distorted cubane topology. (Figure 10)

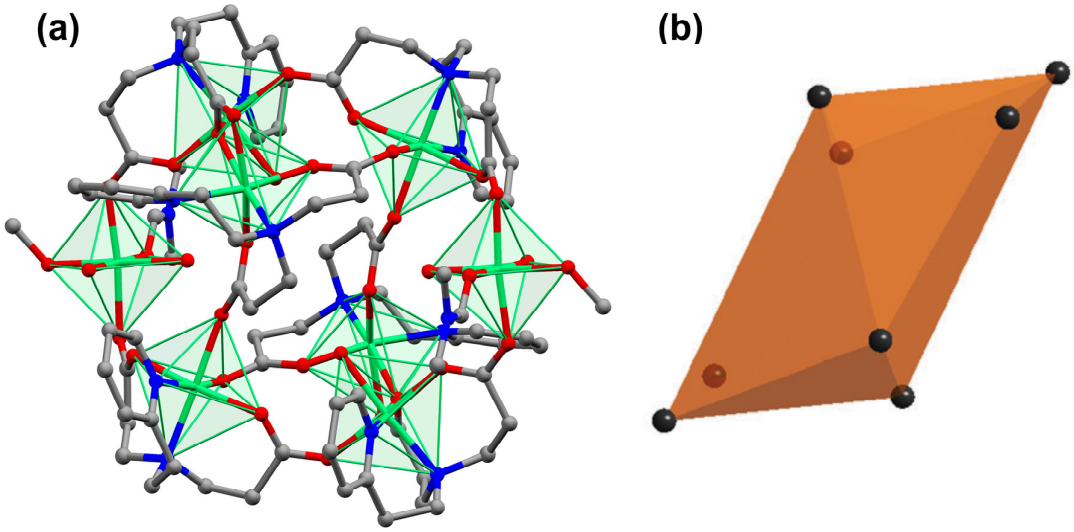


Figure 10. (**a**) Schematic representation of polyhedral view of metal coordination environment in **11**. (**b**) Distorted cubane topology formed by eight nickels center. Color code: green, Ni; blue, N; red, O; and gray, C atoms. Reproduced with permission from ref. [51]. Copyright 2011, Royal Society of Chemistry.

Magnetic measurements (2–300 K) indicate that **11** exhibits overall antiferromagnetic exchange interactions (Figure 11). Six magnetic-exchange coupling constants (J_1 = +0.6, J_2 = +2.4, J_3 = +0.8, J_4 = −24.4, J_5 = +1.4, J_6 = −9.0 cm^{-1}; g = 2.135) were considered based on the geometric parameters of the interacting Ni(II) centers (Scheme 9) [51]. Notably, **11** represents the first Ni_8 cluster that (i) is bridged exclusively by carboxylates in three modes (monodentate, *syn–anti*, and *anti–anti*), (ii) displays four ferromagnetic and two antiferromagnetic interactions, and (iii) shows excellent agreement between the experimentally derived *J* values and those calculated via B3LYP-level DFT [51].

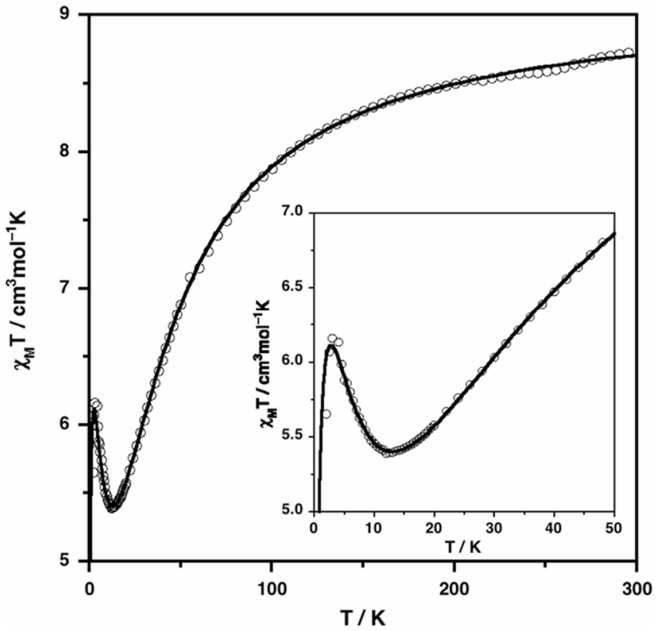
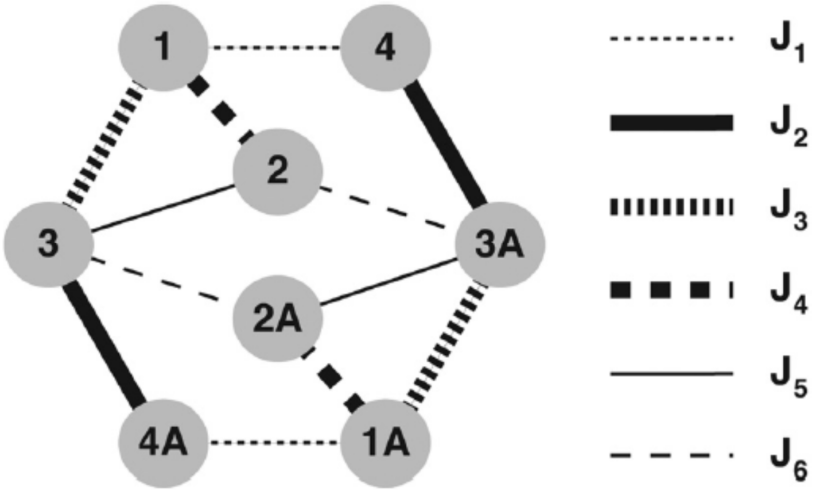


Figure 11. The temperature dependence of $\chi_M T$ for **11**. The inset shows the maximum of $\chi_M T$ for **11**. Reproduced with permission from ref. [51]. Copyright 2011, Royal Society of Chemistry.



Scheme 9. A scheme showing the topology of the spin–spin exchange interactions in cluster **11**. Reproduced with permission from ref. [51]. Copyright 2011, Royal Society of Chemistry.

3.2.4. Dimers

The potential tetradentate ligands $L^5(CO_2Me)_2$ and $L^8(CO_2^-)$ afforded the carboxylate-bridged discrete binuclear coordination complexes $[Cu_2\{(L^5(CO_2)_2)\}_2].CH_3OH.H_2O$ (**13**) [54], $[M_2(L^8(CO_2))_2(CH_3OH)_2](ClO_4)_2$ (M = Mn, **17**; Co, **18**; Ni, **19**; Zn, **20**) [55,56], and $[Cu_2(L^8(CO_2))_2](ClO_4)_2$ (**21**) [55]. Complexes **13** and **17–21** are discrete syn–anti carboxylate-bridged binuclear species with a $\{M^{II}_2(–O–C–O–)_2\}^{2+}$core. The M(II) centers adopt distorted

octahedral MN3O3 geometries in **17–20** and distorted square-pyramidal CuN3O2 geometries in **13** and **21**, coordinated by three nitrogen donors (one pyridyl and two tertiary amines) and two carboxylate oxygens, with methanol additionally coordinating in **17–20**. The structures of $[M_2(L^8(CO_2))_2(CH_3OH)_2](ClO_4)_2$ (M = Mn, **17**, Co, **18**; Ni, **19**; Zn, **20**) are isomorphous. A perspective view of the cationic part of **17** and **21** is displayed in Figure 12. The coordination environment of each Cu(II) ion in **13** and **21** is square pyramidal with coordination by two nitrogens and two carboxylate O atoms of $L^5(CO_2Me)_2$ and a carboxylate O atom belonging to the carboxylate group of the adjacent molecule for **13**, and three nitrogens and a carboxylate O atom of $L^8(CO_2{}^-)$ and a carboxylate O atom belonging to the carboxylate group of an adjacent molecule for **21**. The basal plane comprises N1, N2, O1 and O3 and the apical position is provided by O1# of $L^5(CO_2Me)_2$ for **13** (N1, N2, O1 and O2# and the apical position is provided by the amine N3 of $L^8(CO_2{}^-)$ for **21**). The Cu(II) geometry of the CuN_2O_3 coordination is intermediate, with $\tau = 0.144$ for **13,** while the CuN_3O_2 coordination for **21** is 0.455. Temperature-dependent magnetic susceptibilities for **13**, **17–19**, and **21** revealed very weak antiferromagnetic/ferromagnetic interactions through *syn–anti* carboxylate bridges between the M(II) centers [$J = -8.37$ (6) cm^{-1} (**13**), -1.47 (1) cm^{-1} (**17**), +0.840 (4) cm^{-1} (**18**), +2.95 (1) cm^{-1} (**19**) and -3.43 (1) cm^{-1} (**21**)] [54,55].

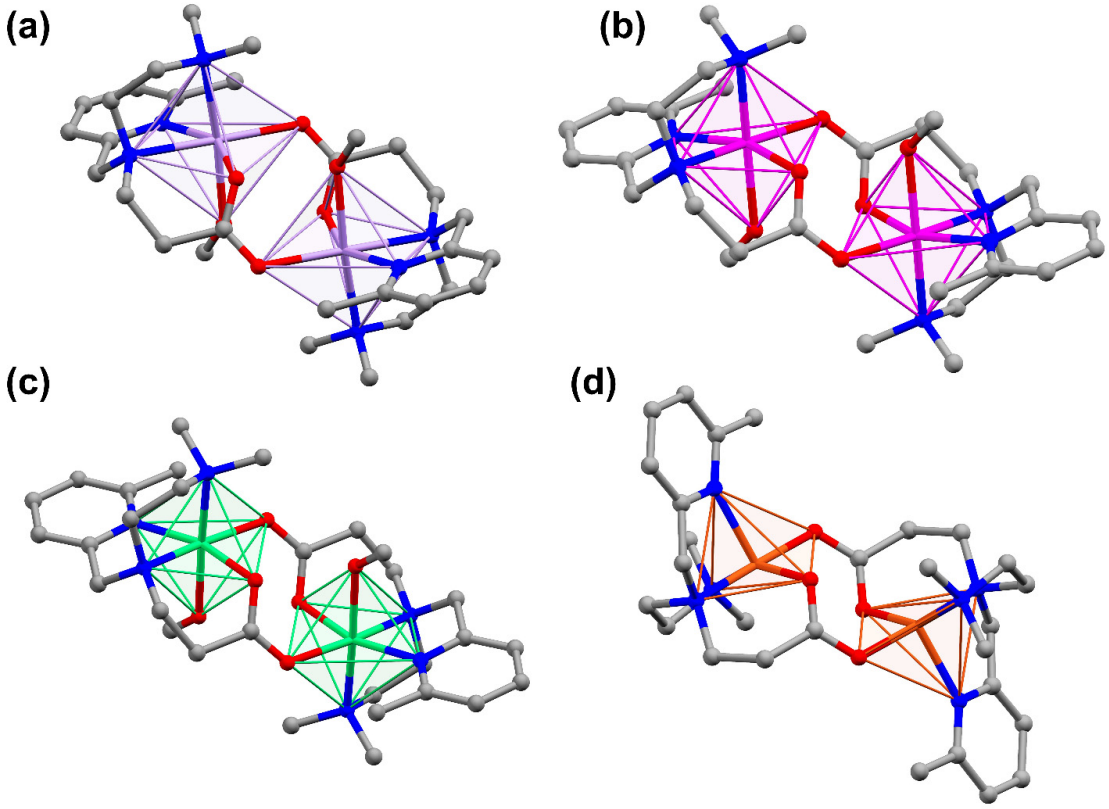


Figure 12. Schematic representation of dinuclear core (**17** (**a**), **18** (**b**), **19** (**c**) and **21** (**d**)). Color code: violet, Mn; blue, pink, Co; green, Ni; orange, Cu; N; red, O; and gray, C atoms. Reproduced with permission from ref. [55]. Copyright 2021, Royal Society of Chemistry.

Variable-temperature magnetic studies of **13**, **17–19**, and **21** reveal that **13** and **17** show antiferromagnetic interactions, while **18**, **19,** and **21** show ferromagnetic interactions. The best-fit parameters are g = 2.11 (1), $J = -8.37$ (6) cm^{-1} for **13**, g = 2.008 (4), $J = -1.47$ (1) cm^{-1} for **17**, g = 2.64 (1), $J = +0.840$ (4) cm^{-1}, D = 78.7 (6) cm^{-1} and $\theta = -0.89$ (1) K for **18**, g = 2.23 (1), $J = +2.95$ (1) cm^{-1}, D = 4.09(3) cm^{-1} for **19,** and g = 2.10 (1), $J = +3.43$ (1) cm^{-1} and $\theta = -0.352$ (3) K for **21** [54,55]. In **18** and **21**, inclusion of a Weiss parameter (θ) was necessary to account for intermolecular antiferromagnetic interactions and accurately re-

produce the low-temperature χ_MT values. For the J value of **13** and that of complexes with similar cores, the extent of antiferromagnetic behavior is strongest in **13**, attesting to the interplay of important structural parameters such as Cu–O and Cu···Cu distances and Cu–O–Cu bridging angles [84–87]. It is a common view that the exchange interaction between two magnetic M(II) ions bridged by the *syn–anti* carboxylate bridge (Scheme 7a) is dominantly weak ferro- or anti-ferromagnetic [88,89]. The magnitude and sign of the exchange interaction (positive for ferromagnetism and negative for antiferromagnetism) [85] depend on the nature of the metal ion (the number and distribution of electrons in the t_{2g} and e_g set of orbitals in octahedral parentage) [88,89]. It was concluded that unpaired electrons in e_g orbitals promote ferromagnetic interactions, whereas those in t_{2g} orbitals lead to stronger antiferromagnetic coupling. Even one unpaired electron in a t_{2g} orbital is enough to dominate the overall magnetic–exchange interaction towards antiferromagnetism [85]. Ferromagnetic interactions are generally predominant in Ni(II) and Cu(II) complexes (with rare exceptions for Cu(II)), whereas Mn(II) and Co(II) systems typically exhibit antiferromagnetic interactions. Thus, the magnetic exchange interactions observed in this work **17** (J = −1.47 (1) cm^{-1}), **18** (J = +0.840 (4) cm^{-1}), **19** (J = +2.95 (1) cm^{-1}) and **21** (J = +3.43 (1) cm^{-1}) closely follow the expected trend [68,90–94]. Although Co(II) complex **18** is anticipated to exhibit antiferromagnetic behavior [90], experimental observations indicate ferromagnetism (Figure 13). However, it should be noted that the magnitude of J (+0.840 (4) cm^{-1}) is very small, and it is slightly correlated with the Weiss parameter, θ = −0.89 K. Moreover, the M–O–C–O–M spin exchange interactions $|J|$ for the dimers of the type $M^{II}_2(OCO)_2$ (M = Mn(3d^5), Co(3d^7), Ni(3d^8), Cu(3d^9)) decrease in strength with $Cu_2(OCO)_2$ > $Ni_2(OCO)_2$ > $Co_2(OCO)_2$ > $Mn_2(OCO)_2$ [87]. The trend observed in this investigation with the same structural topology is consistent with the order reported recently [88]. In complexes with *syn–anti* coordination, the orbital overlap between the bridging ligand and the unpaired electrons on each metal center is expected to be minimal. In this situation, an overall positive value for the coupling constant is expected [93].

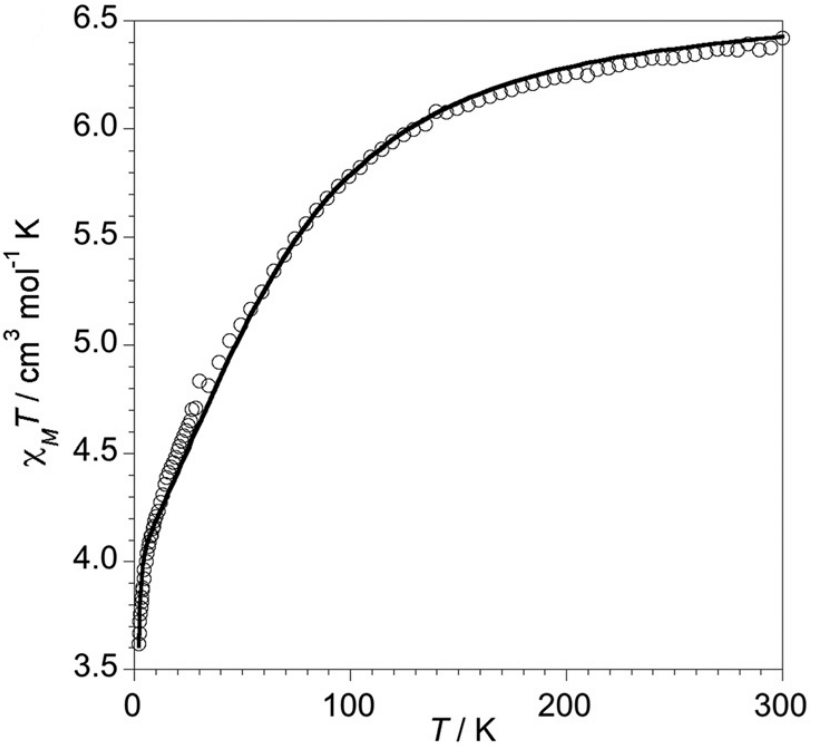


Figure 13. Plot of $\chi_M T$ vs. T for powdered sample of $[Co_2(L^8(CO_2))_2(CH_3OH)_2](ClO_4)_2$ (**18**). Reproduced with permission from ref. [55]. Copyright 2021, Royal Society of Chemistry.

4. Summary and Concluding Remarks

Based on the structural features presented above, one can summarize the following points. (i) Out of the **21** coordination complexes (polymeric or discrete) reported here, **10** have Cu^{II} as the metal ion. (ii) Barring complexes **11** (discrete octanuclear Ni) and **12** (discrete tetranuclear Co), all are linked by syn–anti carboxylate bridges. Complex **11** has anti–anti carboxylate bridges in addition to syn–anti bridges, while complex **12** has only μ-1,1-carboxylate bridges. (iii) All the coordination polymers reported have a 1D layered network. (iv) All tetranuclear coordination complexes reported here, barring **12**, have a 16-membered ring $(–M–O–C–O)_4$ (M = Ni, Cu) structure formed with the carboxylate-bridging groups and four M^{II} ions, where the metal ions are located at the corners of an approximate square plane (see above). This review illustrates that the careful choice of metal–ligand coordination units with diverse geometries enables the construction of coordination clusters (polymeric or discrete) and the exploration of their magnetic behavior. The present review highlights how pyridine–amine–carboxylate ligands serve as versatile molecular tools for directing the self-assembly of both polymeric and discrete coordination clusters with diverse topologies and magnetic behaviors [95–97]. Systematic variations in ligand denticity, flexibility, and steric environment govern metal–ligand connectivity, ultimately shaping nuclearity and overall architecture. The magneto-structural analysis across Mn(II), Co(II), Ni(II) and Cu(II) systems shows that subtle geometric features—particularly the bridging mode of carboxylates—play a decisive role in tuning ferro-, antiferro-, or spin-canted exchange interactions. These insights strengthen the structure–property correlations essential for rational design of next-generation molecular magnetic materials. Continued exploration of modified ligand scaffolds, combined with advanced computational and spectroscopic approaches, will support the discovery of clusters with unprecedented magnetic responses and potential applications in quantum materials, information storage, and molecular spintronics.

Author Contributions: A.R.: Formal analysis, Software, investigation, Data curation, Funding acquisition. A.A.: Kumar: Formal analysis, Software, Data curation. H.A.: Methodology, Conceptualization, Writing—review & editing, Writing—original draft, Supervision, Project administration, A.K.: Conceptualization, Writing—review & editing, Writing—original draft, Supervision, Project administration. All authors have read and agreed to the published version of the manuscript.

Funding: Amit Rajput thanks for Science and Engineering Research Board, New Delhi, India for funding (SUR/2022/001062, SPG/2021/004027), DST PURSE Grant (SR/PURSE/2022/126) to J. C. Bose University of Science & Technology, YMCA, Faridabad, Haryana, Seed Grant (R&D/SG/2023/1589) of J. C. Bose University of Science & Technology, YMCA, Faridabad, Haryana.

Data Availability Statement: Not applicable.

Acknowledgments: Amit Rajput and Akram Ali contributed equally to this work. The authors gratefully acknowledge the contributions of their collaborators and coworkers cited in the references, the constructive and helpful comments of the reviewers during the revision of the manuscript, and the infrastructure support provided by J. C. Bose University of Science and Technology, YMCA, Faridabad, India; the University of Allahabad, Prayagraj, India; and Ewha Womans University, Seoul, Republic of Korea.

Conflicts of Interest: The authors declare no conflicts of interest.

References

1. Bowman-James, K. Alfred Werner revisited: The coordination chemistry of anions. *Acc. Chem. Res.* **2005**, *38*, 671–678. [CrossRef] [PubMed]

2. Cook, T.R.; Zheng, Y.-R.; Stang, P.J. Metal–organic frameworks and self-assembled supramolecular coordination complexes: Comparing and contrasting the design, synthesis, and functionality of metal–organic materials. *Chem. Rev.* **2013**, *113*, 734–777. [CrossRef] [PubMed]
3. Janiak, C. Engineering coordination polymers towards applications. *Dalton Trans.* **2003**, 2781–2804. [CrossRef]
4. Kitagawa, S.; Kitaura, R.; Noro, S.-I. Functional porous coordination polymers. *Angew. Chem. Int. Ed.* **2004**, *43*, 2334–2375. [CrossRef]
5. Chen, C.-T.; Suslick, K.S. One-dimensional coordination polymers: Applications to material science. *Coord. Chem. Rev.* **1993**, *128*, 293–322. [CrossRef]
6. Eddaoudi, M.; Moler, D.B.; Li, H.; Chen, B.; Reineke, T.M.; O'Keeffe, M.; Yaghi, O.M. Modular Chemistry: Secondary Building Units as a Basis for the Design of Highly Porous and Robust Metal−Organic Carboxylate Frameworks. *Acc. Chem. Res.* **2001**, *34*, 319–330. [CrossRef]
7. James, S.L. Metal-organic frameworks. *Chem. Soc. Rev.* **2003**, *32*, 276–288. [CrossRef]
8. Rao, C.N.R.; Natarajan, S.; Vaidhyanathan, R. Metal carboxylates with open architectures. *Angew. Chem. Int. Ed.* **2004**, *43*, 1466–1496. [CrossRef]
9. Gianneschi, N.C.; Masar, M.S.; Mirkin, C.A. Development of a coordination chemistry-based approach for functional supramolecular structures. *Acc. Chem. Res.* **2005**, *38*, 825–837. [CrossRef]
10. Champness, N.R. Coordination frameworks–where next? *Dalton Trans.* **2006**, 877–880. [CrossRef]
11. Kumar, A.; Rajput, A.; Kaur, P.; Verma, I.; Erande, R.D.; Javed, S.; Kłak, J.; Alrebei, S.F.; Mota, A.J.; Colacio, E.; et al. Experimental and theoretical magnetostructural studies on discrete heterometallic cyanide-bridged dinuclear $Fe^{III}Mn^{II}$ and tetranuclear $Fe^{III}{}_2Cu^{II}{}_2$ complexes bearing tripodal pyrazolyl borate and tetradentate phenolate-based ligands. *Dalton Trans.* **2023**, *52*, 7225–7238. [CrossRef]
12. Ahmed, S.; Kumar, A.; Mukhopadhyay, A.; Lloret, F.; Mukherjee, R. Heterobimetallic cyanide-bridged $Fe^{III}(\mu$-CN)M^{II} complexes (M = Mn and Cu): Synthesis, structure and magnetism. *New J. Chem.* **2022**, *46*, 7711–7720. [CrossRef]
13. Fu, J.-H.; Tan, B.-C.; Song, Y.; Wu, Z.-H.; Wu, X.-T.; Sheng, T.-L. Recent developments and challenges of molecular design in linear cyanido-bridged multimetallic complexes. *Dalton Trans.* **2025**, *54*, 4396–4404. [CrossRef] [PubMed]
14. Rajput, A.; Kumar, A.; Sengupta, A.; Tyagi, P.; Arora, H. Copper (II) dimers stabilized by bis(phenol) amine ligands: Theoretical and experimental insights. *New J. Chem.* **2018**, *42*, 12621–12631. [CrossRef]
15. Agarwal, P.; Kumar, A.; Richa; Verma, I.; Erande, R.D.; Kłak, J.; Mota, A.J.; Arora, H.; Rajput, A. The reversible inter-conversion of copper(II) dimers bearing phenolate-based ligands in their monomers: Theoretical and experimental viewpoints. *New J. Chem.* **2021**, *45*, 1203–1215. [CrossRef]
16. Richa; Kumar, A.; Verma, A.; Garg, P.; Erande, R.D.; Javed, S.; Rajput, A.; Garcia, C.J.G.; Mota, A.J.; Arora, H. Magnetic properties and pH-controlled reversible interconversion of μ-oxido into μ-hydroxido in oxo-carboxylato bridged iron(III) dimers: Theoretical and experimental insights. *J. Mol. Struct.* **2023**, *1285*, 135426. [CrossRef]
17. Natarajan, S.; Mandal, S. Open-framework structures of transition-metal compounds. *Angew. Chem. Int. Ed.* **2008**, *47*, 4798–4828. [CrossRef]
18. Perry, J.J., IV; Perman, J.A.; Zaworotko, M.L. Design and synthesis of metal–organic frameworks using metal–organic polyhedral as supermolecular building blocks. *Chem. Soc. Rev.* **2009**, *38*, 1400–1417. [CrossRef]
19. Desiraju, G.R. Crystal engineering. From molecules to materials. *J. Mol. Struct.* **2003**, *656*, 5–15. [CrossRef]
20. Sharma, A.K.; De, A.; Mukherjee, R. Design, structure, and properties of functional metal–ligand inorganic modules. *Curr. Opin. Solid State Mater. Sci.* **2009**, *13*, 54–67. [CrossRef]
21. Ellsworth, J.M.; Zur Loye, H.-C. Metal and mixed-metal coordination polymers synthesized with pyrazine-2-carboxylate. *Dalton Trans.* **2008**, 5823–5835. [CrossRef]
22. Tong, J.; Lu, H.-L.; Sun, W.-Q.; Yu, S.-Y. Design and programmable self-assembly of an eight-coordinate Cu(ii) heterometallic structure via a dipalladium corner as a building block. *Cryst. Eng. Comm.* **2020**, *22*, 8166–8170. [CrossRef]
23. Zhao, N.; Li, Y.; Gu, J.; Fernandes, T.A.; Kirillova, M.V.; Kirillov, A.M. New copper(II) coordination compounds assembled from multifunctional pyridine-carboxylate blocks: Synthesis, structures, and catalytic activity in cycloalkane oxidation. *Molecules* **2019**, *24*, 6. [CrossRef] [PubMed]
24. Deacon, G.B.; Phillips, R.J. Relationships between the carbon-oxygen stretching frequencies of carboxylato complexes and the type of carboxylate coordination. *Coord. Chem. Rev.* **1980**, *33*, 227–250. [CrossRef]
25. Colacio, E.; Domínguez-Vera, J.M.; Ghazi, M.; Kivekäs, R.; Klinga, M.; Moreno, J.M. Singly *anti-anti* carboxylate-bridged zig-zag chain complexes from a carboxylate-containing tridentate schiff base ligand and $M(hfac)_2$ [M = Mn^{II}, Ni^{II}, and Cu^{II}]: Synthesis, crystal structure, and magnetic properties. *Eur. J. Inorg. Chem.* **1999**, *1999*, 441–445. [CrossRef]
26. Colacio, E.; Ghazi, M.; Kivekäs, R.; Moreno, J.M. Helical-chain copper(II) complexes and a cyclic tetranuclear copper(II) complex with single syn-anti carboxylate bridges and ferromagnetic exchange interactions. *Inorg. Chem.* **2000**, *39*, 2882–2890. [CrossRef]
27. Elwell, C.E.; Gangnon, N.L.; Neisen, B.D.; Dhar, D.; Spaeth, A.D.; Yee, G.M.; Tolman, W.B. Copper-oxygen complexes revisited: Structures, spectroscopy and reactivity. *Chem. Rev.* **2017**, *117*, 2059–2107. [CrossRef]

28. Ha, D.; Kumar, A.; Hong, Y.H.; Lee, Y.-M.; Fukuzumi, S.; Nam, W. High oxidizing reactivity of mononuclear nonheme iron(V)-oxo complexes. *J. Inorg. Biochem.* **2025**, *40*, 113143. [CrossRef]
29. Himes, R.A.; Karlin, K.D. Copper–dioxygen complex mediated C–H bond oxygenation: Relevance for particulate methane monooxygenase (pMMO). *Curr. Opin. Chem. Biol.* **2009**, *13*, 119–131. [CrossRef]
30. Maurits de Roo, C.; Klement, W.J.N.; Duijnstee, D.R.; Staykov, A.; Browne, W.R. Seeing an unobservable Fe(III)/Fe(IV) redox process of the nonheme iron N4Py complex by high-speed surface-enhanced raman spectroelectrochemistry. *Inorg. Chem.* **2025**, *64*, 10549–10557. [CrossRef]
31. Lewis, E.A.; Tolman, W.B. Reactivity of dioxygen−copper systems. *Chem. Rev.* **2004**, *104*, 1047–1076. [CrossRef] [PubMed]
32. Itoh, S.; Tachi, Y. Structure and O_2-reactivity of copper(I) complexes supported by pyridylalkylamine ligands. *Dalton Trans.* **2006**, 4531–4538. [CrossRef] [PubMed]
33. Mizuno, M.; Hayashi, H.; Fujinami, S.; Furutachi, H.; Nagatomo, S.; Otake, S.; Uozumi, K.; Suzuki, M.; Kitagawa, T. Ligand effect on reversible conversion between copper(I) and bis(μ-oxo)dicopper(III) complex with a sterically hindered tetradentate tripodal ligand and monooxygenase activity of bis(μ-oxo)dicopper(III) complex. *Inorg. Chem.* **2003**, *42*, 8534–8544. [CrossRef] [PubMed]
34. Komiyama, K.; Furutachi, H.; Nagatomo, S.; Hashimoto, A.; Hayashi, H.; Fujinami, S.; Suzuki, M.; Kitagawa, T. Dioxygen reactivity of copper(I) complexes with tetradentate tripodal ligands having aliphatic nitrogen donors: Synthesis, structures, and properties of peroxo and superoxo complexes. *Bull. Chem. Soc. Jpn.* **2004**, *77*, 59–72. [CrossRef]
35. Shimazaki, Y.; Nogami, T.; Tani, F.; Odani, A.; Yamauchi, O. Effects of a Side Chain Aromatic Ring on the Reactivity of Copper(I) Complexes with Dioxygen. *Angew. Chem. Int. Ed.* **2001**, *40*, 3859–3862. [CrossRef]
36. Sun, L.; Gutierrez, J.; Gatineau, D.; Sanahuges, R.; Curtil, M.; Philouze, C.; Dechert, S.; Demeshko, S.; Jackson, T.A.; Meyer, F.; et al. Non-Heme Tri-Iron(II) Complex as a Precursor for Dioxygen Activation and Oxygen Reduction Reaction Catalysis. *Inorg. Chem.* **2025**, *64*, 16309–16322. [CrossRef]
37. Fujii, T.; Yamaguchi, S.; Hirota, S.; Masuda, H. H-atom abstraction reaction for organic substrates via mononuclear copper(II)-superoxo species as a model for DβM and PHM. *Dalton Trans.* **2008**, 164–170. [CrossRef]
38. Suzuki, M. Ligand effects on dioxygen activation by copper and nickel complexes: Reactivity and intermediates. *Acc. Chem. Res.* **2007**, *40*, 609–617. [CrossRef]
39. Thomas, F. Ten years of a biomimetic approach to the copper(II) radical site of galactose oxidase. *Eur. J. Inorg. Chem.* **2007**, *2007*, 2379–2404. [CrossRef]
40. Tshuva, E.Y.; Lippard, S.J. Synthetic models for non-heme carboxylate-bridged diiron metalloproteins: Strategies and tactics. *Chem. Rev.* **2004**, *104*, 987–1012. [CrossRef]
41. Mukhopadhyay, S.; Mandal, S.K.; Bhaduri, S.; Tolman, W.B. Manganese clusters with relevance to photosystem II. *Chem. Rev.* **2004**, *104*, 3981–4026. [CrossRef]
42. Filipović, N.; Stanković, A.; Medvidović-Kosanović, M.; Goman, D.; Šarić, S.; Palijan, G.; Balić, T. Synthesis, crystallographic study and antibacterial activity of ternary copper(II) complex with chromone-based ligand and pyridine. *Crystals* **2025**, *15*, 870. [CrossRef]
43. Singh, R.; Mukhopadhyay, N.; Lloret, F.; Mukherjee, R. Synthesis and reactivity of a bis(hydroxido)-bridged dicopper(II) complex: Hydrolysis of carboxylate esters and coordination polymer with phosphate diester. *Eur. J. Inorg. Chem.* **2025**, *28*, e202400850. [CrossRef]
44. Rojas, D.; García, A.M.; Vega, A.; Moreno, Y.; Venegas-Yazigi, D.; Garland, M.T.; Manzur, J. Binuclear copper(II) oxidation products from copper(I) complexes with tridentate ligands. Magnetostructural characterization. *Inorg. Chem.* **2004**, *43*, 6324–6330. [CrossRef] [PubMed]
45. Cañon-Mancisidor, W.; Spodine, E.; Venegas-Yazigi, D.; Rojas, D.; Manzur, J.; Alvarez, S. Electrochemical behavior of copper complexes with substituted polypyridinic ligands: An experimental and theoretical study. *Inorg. Chem.* **2008**, *47*, 3687–3692. [CrossRef] [PubMed]
46. Mukherjee, R. *Comprehensive Coordination Chemistry II: From Biology to Nanotechnology*; McCleverty, J.A., Meyer, T.J., Fenton, D.E., Eds.; Chapter on Copper; Elsevier/Pergamon: Amsterdam, The Netherlands, 2004; Volume 6, pp. 747–910.
47. Arora, H.; Lloret, F.; Mukherjee, R. One-dimensional coordination polymers of Mn^{II}, Cu^{II}, and Zn^{II} supported by carboxylate-appended (2-pyridyl)alkylamine ligand– structure and magnetism. *Eur. J. Inorg. Chem.* **2009**, *2009*, 3317–3325. [CrossRef]
48. Arora, H.; Lloret, F.; Mukherjee, R. One-dimensional Co^{II} and Cu^{II} coordination polymers and a discrete Cu^{II}_4 Complex of carboxylate-appended (2-pyridyl)alkylamine ligands: Spin-canting and anti-/ferromagnetic coupling. *Inorg. Chem.* **2009**, *48*, 1158–1167. [CrossRef]
49. Arora, H.; Lloret, F.; Mukherjee, R. Molecular squares of Ni^{II} and Cu^{II}: Ferromagnetic exchange interaction mediated by syn–anticarboxylate-bridging. *Dalton Trans.* **2009**, 9759–9769. [CrossRef]
50. Arora, H.; Cano, J.; Lloret, F.; Mukherjee, R. Unprecedented heptacopper(II) cluster with body-centred anti-prismatic topology. Structure, magnetism and density functional study. *Dalton Trans.* **2011**, *40*, 10055–10062. [CrossRef]
51. Arora, H.; Cano, J.; Lloret, F.; Mukherjee, R. A carboxylate-bridged NiII8 cluster with a distorted cubane topology: Structure, magnetism and density functional studies. *Dalton Trans.* **2016**, *45*, 14174–14183. [CrossRef]

52. Choi, K.-Y.; Jeon, Y.-M.; Ryu, H.; Oh, J.-J.; Lim, H.-H.; Kim, M.-W. Synthesis and characterization of *syn–anti* carboxylate-bridged one-dimensional copper(II) complexes with bis(2-pyridylmethyl)amino acids. *Polyhedron* **2004**, *23*, 903–911. [CrossRef]
53. Kant, S.; Saha, S.; Lloret, F.; Cano, J.; Mukherjee, R. A tetracobalt(II) cluster with a two vertex truncated dicubane topology endogenously supported by carboxylate-based (2-pyridyl)methylamine ligands: Magneto-structural and DFT studies. *Dalton Trans.* **2023**, *52*, 11922–11933. [CrossRef]
54. Kant, S.; Manda, M.; Mukhopadhyay, N.; Arora, H.; Verma, I.; Lloret, F.; Mukherjee, R. Magneto-structural studies on $[Cu^{II}_2\{L^3\text{-}(\mu_2\text{-}1,1\text{-}CO_2^-)_2\}_2]\bullet MeOH\bullet H_2O$ and $[Cu^{II}_4\{L^4\text{-}(\mu_2\text{-}1,3\text{-}CO_2^-)(\mu_2\text{-}1,3\text{-}CO_2Me)\}_4](ClO_4)_4$ using carboxylate-/carboxymethylester-appended (2-pyridyl)-alkylamine ligands differing in alkyl chain length. *Polyhedron* **2023**, *245*, 116652. [CrossRef]
55. Manda, M.; Arora, H.; Sengupta, A.; Kant, S.; Lloret, F.; Mukherjee, R. Dimeric Mn(II), Co(II), Ni(II) and Cu(II) complexes of a common carboxylate-appended (2-pyridyl)alkylamine ligand: Structure, magnetism and DFT study. *New J. Chem.* **2021**, *45*, 16019–16029. [CrossRef]
56. Kaur, P.; Verma, I.; Khanum, G.; Siddiqui, N.; Javed, S.; Arora, H. Dimeric ZnII complex of carboxylate-appended (2-pyridyl)alkylamine ligand and exploration of experimental, theoretical, molecular docking and electronic excitation studies of ligand. *J. Mol. Struct.* **2023**, *1276*, 134715. [CrossRef]
57. Addison, A.W.; Rao, T.N.; Reedijk, J.; Rijn, J.V.; Verschoor, G.C. Synthesis, structure, and spectroscopic properties of copper(II) compounds containing nitrogen–sulphur donor ligands; the crystal and molecular structure of aqua [1,7-bis(*N*-methylbenzimidazol-2′-yl)-2,6-dithiaheptane]copper(II) perchlorate. *J. Chem. Soc. Dalton Trans.* **1984**, 1349–1356. [CrossRef]
58. Rueff, J.-M.; Masciocchi, N.; Rabu, P.; Sironi, A.; Skoulios, A. Structure and magnetism of a polycrystalline transition metal soap—$Co^{II}[OOC(CH_2)_{10}COO](H_2O)_2$. *Eur. J. Inorg. Chem.* **2001**, *2001*, 2843–2848. [CrossRef]
59. Montney, M.R.; LaDuca, R.L. Structure and magnetic properties of a copper malonate/dipyridylamine layered coordination polymer with both *syn–anti* and *anti–anti* copper carboxylate chains. *Inorg. Chem. Commun.* **2007**, *10*, 1518–1522. [CrossRef]
60. Kahn, O. *Molecular Magnetism*; VCH: New York, UK, 1993.
61. Carlin, R.L. *Magnetochemistry*; Springer: Berlin, Germany, 1986.
62. Li, J.-R.; Yu, Q.; Tao, Y.; Bu, X.-H.; Ribas, J.; Batten, S.R. Magnetic canting or not? Two isomorphous 3D Co^{II} and Ni^{II} coordination polymers with the rare non-interpenetrated (10,3)-d topological network, showing spin-canted antiferromagnetism only in the Co^{II} system. *Chem. Commun.* **2007**, 2290–2292. [CrossRef]
63. Kurmoo, M. Magnetic metal–organic frameworks. *Chem. Soc. Rev.* **2009**, *38*, 1353–1379. [CrossRef]
64. Rodriguez-Martín, Y.; Ruiz-Pérez, C.; Sánchiz, J.; Lloret, F.; Julve, M. Crystal structure and magnetic properties of the flexible self-assembled two-dimensional square network complex $[Cu_2(mal)_2(H_2O)_2(4,4'\text{-bpy})]$ (H_2mal=malonic acid and 4,4′-bpy=4,4′-bipyridine). *Inorg. Chim. Acta* **2001**, *318*, 159–165. [CrossRef]
65. Rodriguez-Martín, Y.; Hernández-Molina, M.; Delgado, F.S.; Pasán, J.; Ruiz-Pérez, C.; Sánchiz, J.; Lloret, F.; Julve, M. Structural versatility of the malonate ligand as a tool for crystal engineering in the design of molecular magnets. *CrystEngComm* **2002**, *4*, 522–535. [CrossRef]
66. Rodriguez-Martín, Y.; Hernández-Molina, M.; Delgado, F.S.; Pasán, J.; Ruiz-Pérez, C.; Sánchiz, J.; Lloret, F.; Julve, M. The flexibility of molecular components as a suitable tool in designing extended magnetic systems. *CrystEngComm* **2002**, *4*, 440–446. [CrossRef]
67. Delgado, F.S.; Sánchiz, J.; Ruiz-Pérez, C.; Lloret, F.; Julve, M. Design of high-dimensional copper(II) malonate complexes with exo-polydentate N-donor ligands. *Inorg. Chem.* **2003**, *42*, 5938–5948. [CrossRef] [PubMed]
68. Rodríguez-Fortea, A.; Alemany, P.; Alvarez, S.; Ruiz, E. Exchange coupling in carboxylato-bridged dinuclear copper(II) compounds: A density functional study. *Chem. Eur. J.* **2001**, *7*, 627–637. [CrossRef]
69. Colacio, E.; Costes, J.-P.; Kivekäs, R.; Laurent, J.-P.; Ruiz, J. A quasi-tetrahedral tetracopper cluster with syn-anti bridging carboxylate groups: Crystal and molecular structure and magnetic properties. *Inorg. Chem.* **1990**, *29*, 4240–4246. [CrossRef]
70. Colacio, E.; Dominguez-Vera, J.-M.; Costes, J.-P.; Kivekäs, R.; Laurent, J.-P.; Ruiz, J.; Sundberg, M. Structural and magnetic studies of a syn-anti carboxylate-bridged helix-like chain copper(II) complex. *Inorg. Chem.* **1992**, *31*, 774–778. [CrossRef]
71. Wang, S.; Trepanier, S.J.; Zheng, J.-C.; Pang, Z.; Wagner, M.J. Homonuclear and heteronuclear metal complexes with a cyclic tetracopper(II) unit. Syntheses, crystal structures, and magnetic properties of $[Cu^{II}_4(dmap)_3(OH)(O_2CCH_3)_2(HO_2CCH_3)(H_2O)][PF_6]_2$,$[Cu^{II}_4(dmap)_2(O_2CCH_3)_4](PF_6)_2$, $[Cu^{II}_4(dmap)_2(O_2CCH_3)_2(OH)_2][Hg^{II}(O_2CCH_3)Cl_2]2[Hg^{II}Cl_2]$, and $[Cu^{II}_4(dmap)_2(O_2CCH_3)_3(OH)_2(H_2O)][PF_6]$ (dmap = 1,3-bis(dimethylamino)-2-propanolato). *Inorg. Chem.* **1992**, *31*, 2118.
72. Murugesu, M.; Clérac, R.; Pilawa, B.; Mandel, A.; Anson, C.E.; Powell, A.K. Ferromagnetic interactions mediated by syn/anti carboxylate bridging in tetranuclear copper(II) compounds. *Inorg. Chim. Acta* **2002**, *337*, 328–336. [CrossRef]
73. Dey, S.K.; Bag, B.; Abdul Malik, K.M.; Salah El Fallah, M.; Ribas, J.; Mitra, S. A Quasi-tetrahedral Cu_4 cluster and a helical-chain copper(II) complex with single syn—anti carboxylate bridges: Crystal structure and magnetic properties. *Inorg. Chem.* **2003**, *42*, 4029–4035. [CrossRef]
74. Cano, J. *VPMAG*; revison B1; University of Valencia: Valencia, Spain, 2003.
75. Angeli, C.; Cimiraglia, R.; Malrieu, J.-P. N-electron valence state perturbation theory: A fast implementation of the strongly contracted variant. *Chem. Phys. Lett.* **2001**, *350*, 297–305. [CrossRef]

76. Angeli, C.; Cimiraglia, R.; Malrieu, J.-P. n-electron valence state perturbation theory: A spinless formulation and an efficient implementation of the strongly contracted and of the partially contracted variants. *J. Chem. Phys.* **2002**, *117*, 9138–9153. [CrossRef]
77. Angeli, C.; Cimiraglia, R.; Evangelisti, S.; Leininger, T.; Malrieu, J.-P. Introduction of n-electron valence states for multireference perturbation theory. *J. Chem. Phys.* **2001**, *114*, 10252–10264. [CrossRef]
78. Ruiz, E.; Rodríguez-Fortea, A.; Cano, J.; Alvarez, S.; Alemany, P. About the calculation of exchange coupling constants in polynuclear transition metal complexes. *J. Comput. Chem.* **2003**, *24*, 982–989. [CrossRef]
79. Ruiz, E.; Cano, J.; Alvarez, S.; Alemany, P. Magnetic coupling in end-on azido-bridged transition metal complexes: Adensity functional Study. *J. Am. Chem. Soc.* **1998**, *120*, 11122–11129. [CrossRef]
80. Kambe, K. On the Paramagnetic Susceptibilities of Some Polynuclear Complex Salts. *J. Phys. Soc. Jpn.* **1950**, *5*, 48–51. [CrossRef]
81. Solomon, E.I.; Chen, P.; Metz, M.; Lee, S.-K.; Palmer, A.E. Oxygen Binding, Activation, and Reduction to Water by Copper Proteins. *Angew. Chem. Int. Ed.* **2001**, *40*, 4570–4590. [CrossRef]
82. Khanra, S.; Weyhermüller, T.; Chaudhuri, P. A nonanuclear copper(II) cluster incorporating endogenous alkoxo- and exogenous hydroxo bridges containing [$Cu_3(\mu_3$-OH)] cores. *Dalton Trans.* **2009**, 3847–3853. [CrossRef]
83. Contaldi, S.; Di Nicola, C.; Garau, F.; Karabach, Y.Y.; Martins, L.M.D.R.S.; Monari, M.; Pandolfo, L.; Pettinari, C.; Pombeiro, A.J.L. New coordination polymers based on the triangular $[Cu_3(\mu_3$-OH)$(\mu$-pz$)_3]^{2+}$ unit and unsaturated carboxylates. *Dalton Trans.* **2009**, 4928–4941. [CrossRef]
84. Greenway, A.M.; O'Connor, C.J.; O'Connor, J.W.; Overman, J.W.; Sinn, E. Magnetic properties and crystal structure of an acetate-bridged ferromagnetic copper(II) dimer. *Inorg. Chem.* **1981**, *20*, 1508–1513. [CrossRef]
85. Chiari, B.; Helms, J.H.; Piovesana, O.; Tarantelli, T.; Zanazzi, P.F. Exchange interaction in multinuclear transition-metal complexes. 9. Magnetostructural correlations in one-atom acetato-bridged copper(II) dimers. *Inorg. Chem.* **1986**, *25*, 2408–2413. [CrossRef]
86. Costas, J.-P.; Dahan, F.; Laurent, J.-P. A further example of a dinuclear copper(II) complex involving monoatomic acetate bridges. Synthesis, crystal structure, and spectroscopic and magnetic properties of bis(.mu.-acetato)bis(7-amino-4-methyl-5-aza-3-hepten-2-onato(1-))dicopper(II). *Inorg. Chem.* **1985**, *24*, 1018–1022. [CrossRef]
87. Arora, H.; Mukherjee, R. Coordination polymers using (2-pyridyl)alkylamine-appended carboxylates: Magnetic properties. *New J. Chem.* **2010**, *34*, 2357–2365. [CrossRef]
88. Su, F.; Lu, L.; Feng, S.; Zhu, M.; Gao, Z.; Dong, Y. Synthesis, structures and magnetic properties in 3d-electron-rich isostructural complexes based on chains with sole *syn–anti* carboxylate bridges. *Dalton Trans.* **2015**, *44*, 7213–7222. [CrossRef] [PubMed]
89. Coronado, E.; Galán-Mascarós, J.R.; Gómez-García, C.; Murcia-Martínez, J.A. Chiral molecular magnets: Synthesis, structure, and magnetic behavior of the series [M (L-tart)] (M = Mn^{II},Fe^{II},Co^{II},Ni^{II}; L-tart = (2R,3R)-(+)-tartrate). *Chem. Eur. J.* **2006**, *12*, 3484–3492. [CrossRef]
90. Chen, Z.; Li, Y.; Jiang, C.; Liang, F.; Song, Y. Metal complexes with *N*-(2-pyridylmethyl)iminodiacetate: From discrete polynuclear compounds to 1D coordination polymers. *Dalton Trans.* **2009**, 5290–5299. [CrossRef]
91. Durot, S.; Policar, C.; Pelosi, G.; Bisceglie, F.; Mallah, T.; Mahy, J.-P. Structural and magnetic properties of carboxylato-bridged manganese(II) complexes involving tetradentate ligands: Discrete complex and 1D polymers. Dependence of *J* on the nature of the carboxylato bridge. *Inorg. Chem.* **2003**, *42*, 8072–8080. [CrossRef]
92. Policar, C.; Lambert, M.; Cesario, M.; Morgenstern-Badarau, I. An Inorganic helix $[Mn(IPG)(MeOH)]_n[PF_6]_n$: Structural and magnetic properties of a *syn-anti* carboxylate-bridged manganese(II) chain involving a tetradentate ligand. *Eur. J. Inorg. Chem.* **1999**, *1999*, 2201–2207. [CrossRef]
93. Du, M.; Bu, X.-H.; Guo, Y.-M.; Zhang, L.; Liao, D.-Z.; Ribas, J. First tetrameric Ni^{II} cluster with planar triangular topology exhibiting ferromagnetic pathways. *Chem. Commun.* **2002**, 1478–1479. [CrossRef]
94. Delgado, F.S.; Hernández-Molina, M.; Sanchiz, J.; Ruiz-Pérez, C.; Rodríguez-Martín, Y.; López, T.; Lloret, F.; Julve, M. Synthesis, crystal structure and magnetic properties of two dimensional malonato-bridged cobalt(II) and nickel(II) compounds. *CrystEngComm* **2004**, *6*, 106–111. [CrossRef]
95. Luneau, D. Molecular magnets. *Curr. Opin. Solid State Mater. Sci.* **2001**, *5*, 123–129. [CrossRef]
96. Verdaguer, M. Rational synthesis of molecular magnetic materials: A tribute to Olivier Kahn. *Polyhedron* **2001**, *20*, 1115–1128. [CrossRef]
97. Coronado, E.; Dunbar, K.R. Preface for the forum on molecular magnetism: The role of inorganic chemistry. *Inorg. Chem.* **2009**, *48*, 3293–3295. [CrossRef]

Disclaimer/Publisher's Note: The statements, opinions and data contained in all publications are solely those of the individual author(s) and contributor(s) and not of MDPI and/or the editor(s). MDPI and/or the editor(s) disclaim responsibility for any injury to people or property resulting from any ideas, methods, instructions or products referred to in the content.